NTNU – Trondheim
Norwegian University of
Science and Technology

Analysis of an Impedance Model for Porous Semiconductor Electrodes

Johanna Etilde Marie Hansen

Abstract

The main aim of this work was to analyze an impedance model for porous semiconductor electrodes consisting of spherical particles. The model should make it possible to analyze the flatband potential for this type of electrodes. The analysis was conducted by simulating the model in MATLAB®. Cyclic voltammetry and electrochemical impedance spectroscopy was performed on titanium oxide, TiO_2 P25, anodized titanium and some iridium tin oxides, $Ir_{(1-x)}Sn_xO_2$. The aim was to use the experimental data as a reference and compare the simulated data with the experimental results. This could not be done because the recorded data for the oxides were too strongly influenced by the support material. The supports tested in this work were Au, Ti and ITO. The simulations show that the capacitance of the models spherical particle is only weakly dependent on the particles surface potential. This indicates that this one-dimensional version of the model might not be sufficient to analyze the spherical particles. However, another analysis method for investigation of Mott-Schottky behavior for porous electrodes was confirmed by the result for the anodized titanium.

Sammendrag

Hovedformålet med dette arbeidet var å analysere en impedans modell for porøse halvleder-elektroder bestående av sfæriske partikler. Modellen skal gjøre det mulig å analysere flatbåndpotensialet for denne typen elektroder. Analysen ble gjennomført ved å simulere modellen i MATLAB®. Syklisk voltammetri og elektrokjemisk impedans spektroskopi ble utført på titanoksid (TiO_2 P25), anodisert titan og utvalgte iridiumtinnoksider, $Ir_{(1-x)}Sn_xO_2$. Målet var å bruke eksperimentelle data som en referanse og sammenligne simulerte data med de eksperimentelle resultatene. Dette ble ikke mulig. De eksperimentelle målingene for oksidfilmene var i for stor grad påvirket av elektrode substratet. Substratene som ble testet i løpet av arbeidet var Au, Ti og ITO. Simuleringene av modellen viser at kapasitansen til de sfærisk partiklene kun er svakt avhengig av det påtrykte overflatepotensial. Dette indikerer at den en-dimensjonal versjon av modellen ikke er tilstrekkelig til å analysere sfæriske partikler. En annen analysemetode for undersøkelse av Mott-Schottky oppførsel for porøse elektroder ble imidlertid bekreftet av de eksperimentelle resultatene for anodisert titan.

Acknowledgements

Contents

1 Introduction

Electrochemical impedance spectroscopy is an important tool in electrochemistry. During this method the electrochemical cell is exited by a sinusoidal potential signal, while the resulting current is measured. The recorded data can be used in a variety of analysis methods. In addition to data about electrode kinetics and adsorption properties, the method can give other useful information. This can be information about corrosion processes, battery properties, aging of sensors and the properties of porous electrodes [1].

Although electrochemical impedance spectroscopy is a widely used and developed technique, it is not jet fully capable as a tool to analyse semiconductor electrodes. Until recent decades semiconductor electrochemistry has been dominated by measurements on planar single-crystals. In the last couple of decades however, the interest has shifted towards porous systems, e.g. electrodes comprised of, more or less, tightly packed particles [2].

A significant aspect in characterization of semiconductor electrodes is the analysis of the flatband potential from Mott-Schottky plots. For systems with small particle size this theory is assumed to be invalid because of the lack of a sustained depletion layer. For larger particles however, it might be possible to utilize the Mott-Schottky theory. With this assumption and results from previous work on porous electrodes [3] as a basis, an impedance model for porous semiconductor electrodes has been derived by Sunde and Tjelta [2]. The model will, if successful, yield a means to analyse the Mott-Schottky behaviour of porous electrodes parallel to the current analysis possible for planar electrodes.

The aim of this thesis is to analyse the derived model and determine if it is possible to extract information about the flatband potential from impedance measurements on porous semiconductor electrodes. This will be done by simulating the impedance model in MATLAB® and comparing the results with impedance data obtained through experiments performed on the widely examined semiconductor, TiO_2 P25. In addition, experiments will be performed on anodically formed TiO_2, and iridium tin oxides, $Ir_{(1-x)}Sn_xO_2$.

2 Theory

This chapter gives a short introduction of the characterization methods used in the experimental work. In addition, the main theory behind the impedance model for porous semiconducting electrodes, derived by Sunde and Tjelta [2], is presented. Some of the mathematical tools used in the model are also described.

2.1 Electrochemical characterization methods

2.1.1 Cyclic voltammetry

During cyclic voltammetry the potential of the electrode to be studied is varied cyclically, while the current response is recorded. The voltage is changed with a constant sweep rate, v, between two potential limits, *Ea* and *Ec*, representing the anodic and the cathodic turning point, respectively. Most commonly the potential is swept between the decomposition potentials of the solvent used in the experiment. For aqueous solutions the onset potentials of hydrogen and oxygen evolution are often chosen as turning points, but in special cases other limits may be used. The sweep rates can range from a few mVs^{-1} up to 10^3- 10^4 Vs^{-1} [4]. Figure 2.1[4] show a typical voltammogram for a Pt-electrode measured in 1M H_2SO_{4-} solution. Since there are no redox-active species in the solution the peaks in the voltammogram represents the adsorption and desorption of oxygen and hydrogen on the electrode surface. In the anodic part of the sweep, the peaks between 0 and 450 mV are due to the oxidation of hydrogen gas near the electrode and desorption of chemisorbed hydrogen. Above 450 mV a constant current flows through the cell and this corresponds to the charging of the electrolytic double layer. The relationship between the current density and the surface capacitance in this area is $i_c = C_D \cdot v$ and $v = dE/dt$ [1].
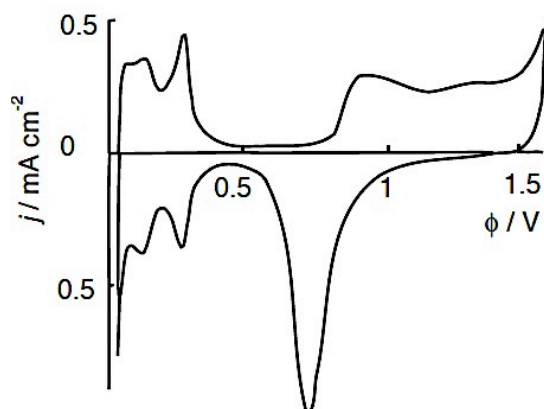
Figure 2.1: Cyclic voltammogram for a Pt-electrode in 1.0 M H_2SO_4 [4].

At potentials above 800 mV peaks corresponding to the chemisorption of oxygen appears. First to take place is the chemisorption of hydroxide, then as the potential increases further oxidation resulting in chemisorbed oxygen. If the potential reaches values above 1600 mV oxygen evolution will occur.

For metallic electrodes, the shape of the voltammogram is mainly dependent on the type of metal and not so much the electrolyte used in the cell [1]. This can be utilized to identify which material dominates the measurements in e.g. the case of powder electrodes deposited on metallic support materials.

2.1.2 Electrochemical Impedance Spectroscopy

During electrochemical impedance spectroscopy a sinusoidally varying potential is applied to the interface, often in addition to a constant direct potential. The alternating potential applied to the system is time dependent and can be written as in Eq. (2.1) [5].

$$E(t) = \Delta E \cdot sin(\omega t) \tag{2.1}$$

$E(t)$ is the instantaneous value and ΔE is the maximum amplitude of the applied sinusoidal potential. The angular frequency is $\omega = 2\pi f$, where f is the frequency of the applied signal. The amplitude of the alternating potential should be kept small, i.e. below ±10 mV [6, 7] and is usually set between 5-10 mV[3]. This is because most electrochemical systems behaves linearly at signal amplitude of 10 mV or less [8].

The resulting current is usually also a sinusoidal signal and of the same frequency as the applied potential. This can be written as in Eq. (2.2) [5].

$$i(t) = \Delta i \cdot sin(\omega t + \phi) \tag{2.2}$$

Δi is the maximum amplitude and ϕ is the phase difference between the applied voltage and the resulting current. It is often convenient to think of the voltages and currents as rotating vectors and to represent them in a phasor plane. Figure 2.2 shows a phasor diagram for a voltage and current phasor separated by the phase angle ϕ [5].
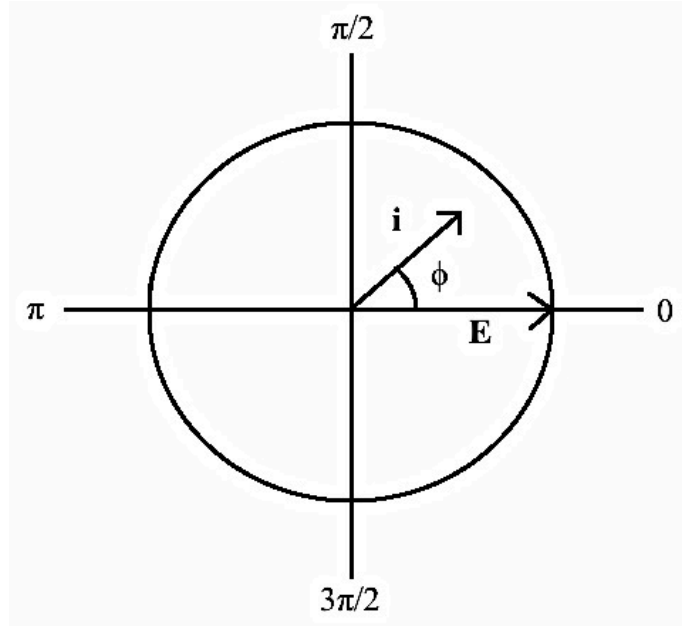
Figure 2.2: Phasor diagram showing the current and voltage phasors separated by the phase angle ϕ. Figure is copied from [5].

The impedance of an electrochemical system is defined as the ratio between the alternating potential and the resulting current according to Eq. (2.3) [8], where the impedance is expressed as a complex vectors.

$$\tilde{Z} = \frac{\tilde{E}(t)}{\tilde{\iota}(t)} = |Z| \exp(j\phi) = ReZ + j \cdot ImZ \qquad (2.3)$$

Here *ReZ* is the real part of the complex impedance, $j = \sqrt{-1}$ is the complex number and *ImZ* is the imaginary part. The impedance can be measured over a wide range of frequencies to make an impedance spectrum, *Z(ω)* [4], which can ranges from 1mHz up to 10MHz [8], and can be recorded at several different steady state potentials.

An electrochemical cell can be modelled as an equivalent circuit consisting of a combination of circuit elements like resistances, capacitors or inductances, but also some mathematical components [8]. Each circuit element has a corresponding impedance, *X*, and the phase angle for each element can be found using Eq. (2.4), in which *R* is the resistance [5].

$$\tan \phi = \frac{X}{R} \qquad (2.4)$$

For a regular resistance, *R*, the phase angle $\phi = 0$ and the impedance is simply given by [5]

4

$$X_R = R \qquad\qquad (2.5)$$

In the case of a capacitor $\phi = \pi/2$ and the impedance can be expressed as in Eq. (2.6)[6]. The phase angle for an inductor is $\phi = -\pi/2$ and the impedance is given in Eq. (2.7) [6].

$$X_C = \frac{1}{j\omega C} \qquad\qquad (2.6)$$

$$X_L = j\omega L \qquad\qquad (2.7)$$

Here C is the capacitance and L is the inductance.

Most electrochemical systems consist of several circuit elements connected in parallel and series. The total impedance of a system can be calculated using the same rules as for common resistors connected in a circuit. The total impedance of two impedances in series can be calculated from Eq. (2.8)[6], while the total impedance for two impedances in parallel is found using Eq. (2.9) [6].

$$Z_{tot} = Z_1 + Z_2 \qquad\qquad (2.8)$$

$$1/Z_{tot} = 1/Z_1 + 1/Z_2 \qquad\qquad (2.9)$$

The equivalent circuit for a simple electron transfer reactions can be seen in Figure 2.3(a) [1]. The circuit elements R_E and R_{CT} are the electrolytes resistance and the charge transfer resistance, respectively. C_D is the double layer capacitance. The figure also shows, in (b), the Nyquist-diagram in which $-ImZ$ is plotted as a function of ReZ.
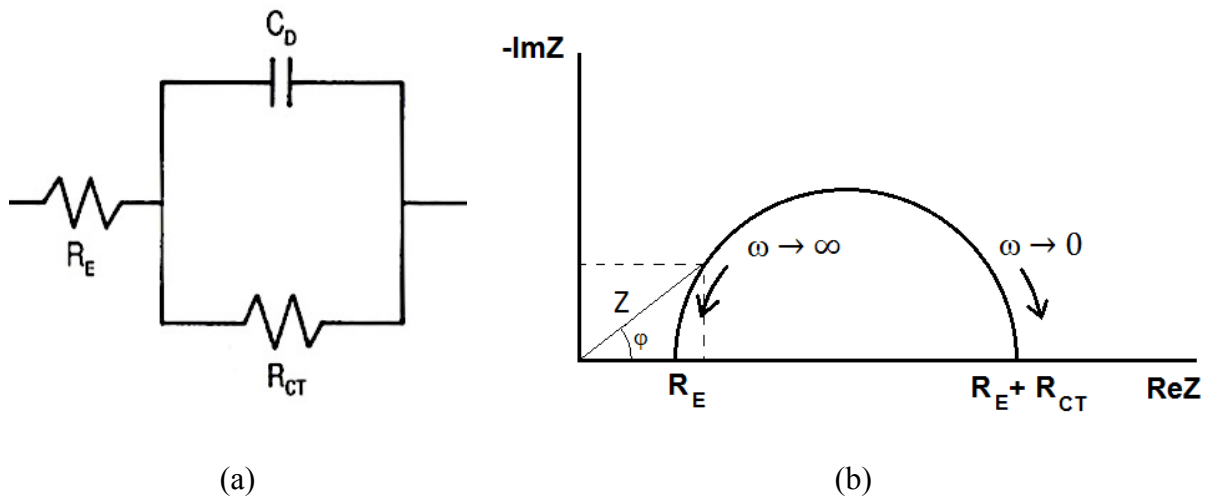
Figure 2.3: Equivalent circuit for a simple electron transfer (a)[1] and the corresponding Nyquist diagram (b), which is copied from [1].

In Figure 2.3, diffusion of species in the electrolyte is neglected. If this effect is included in addition to the charge transfer reaction, the circuit can be sketched as in Figure 2.4. The additional element in the parallel is the Walburg-impedance, which comprises a resistance and capacitor in series [1]. This result in the Nyquist-diagram shown in Figure 2.5, where the effect of the Walburg-impedance is clearly visible in the low frequency area of the curve, marked as the Walburg slope.
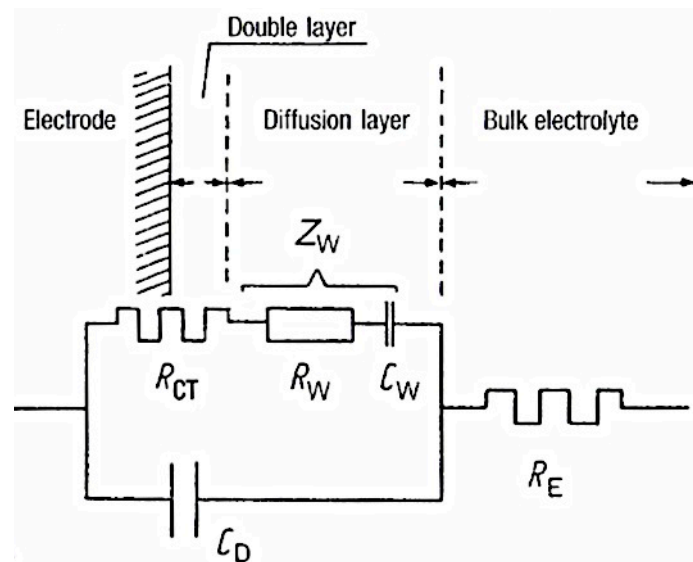
Figure 2.4:The equivalent circuit where both the charge transfer and diffusion in the electrolyte is included [1].
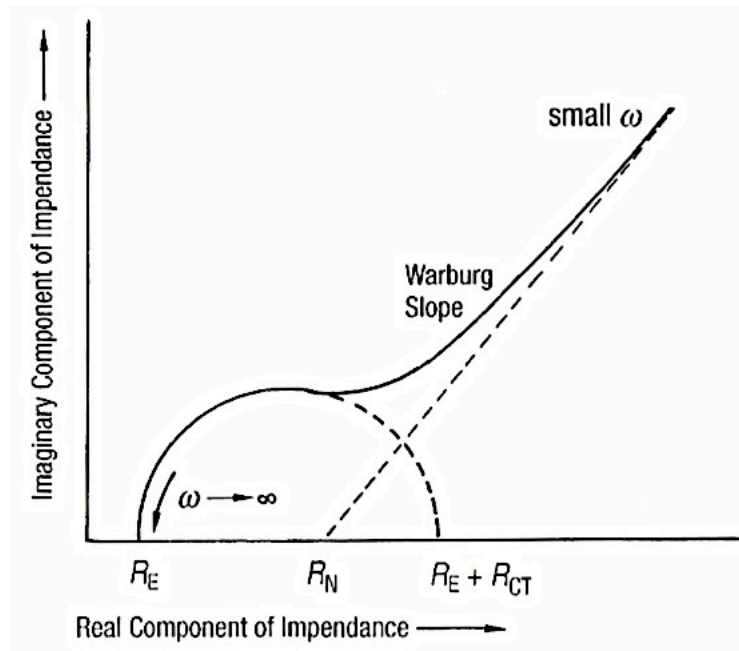
Figure 2.5: The Nyquist diagram[1] for the equivalent circuit in Figure 2.4. The diagram shows mixed control, the charge transfer controls the high frequency area and diffusion controls the low frequency area.

There are a number of ways to present impedance data in addition to the Nyquist-diagram. When working with porous electrodes, it is convenient to plot a logarithmic plot the imaginary impedance, *ImZ*, as a function of the angular frequency, ω, as illustrated in Figure 2.6. This yields information about the electrodes structure. Planar electrodes will result in plots where the linear part of the curve has a slope of -1, while the slope will be -1/2 for a porous electrode. In Bode-diagrams, the absolute value of the total impedance and the phase angle are plotted as a function of the angular frequency, in a logarithmic and semi-logarithmic plot, respectively.

7
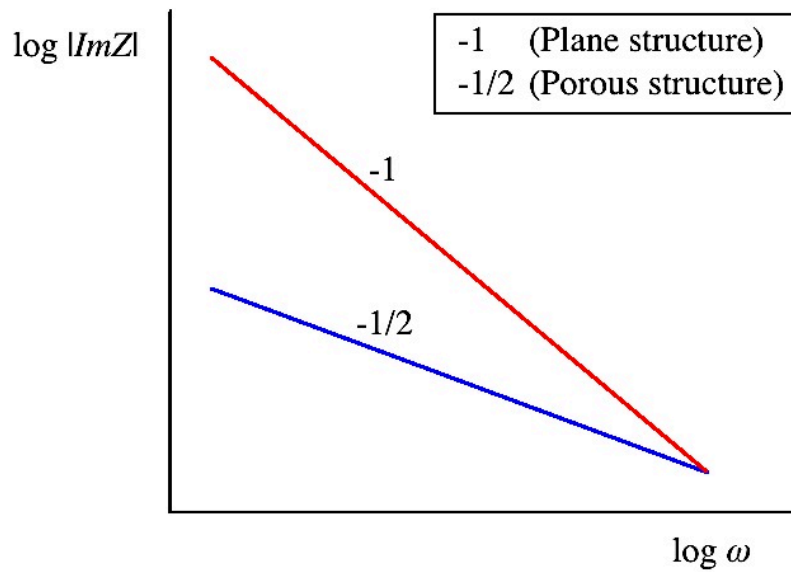
Figure 2.6: Logarithmic plot of the imaginary part of the impedance, *ImZ*, as a function of the angular frequency, ω. Straight lines with a slope of about -1 indicate that the electrode has a planar structure. Lines with a slope close to -1/2 indicate a porous structure.

2.1.3   Impedance for porous electrodes

Electrochemical impedance spectroscopy is a method with high sensitivity to interfacial processes and surface geometry. While the equivalent circuit for planar electrodes may be fairly simple, they are far more complex for porous electrodes The impedance in a single cylindrical pore, with pore length, *l*, and radius, r_{pore}, cannot be represented by a simple connection of capacitors, inductors and resistances. It must be represented by a transmission line [9]. This is a semi-infinite series like the one represented in Figure 2.7. In the figure, R_{pore} is the ohmic resistance of the pore, while C_D is the double layer capacitance for a small element of the pore length.
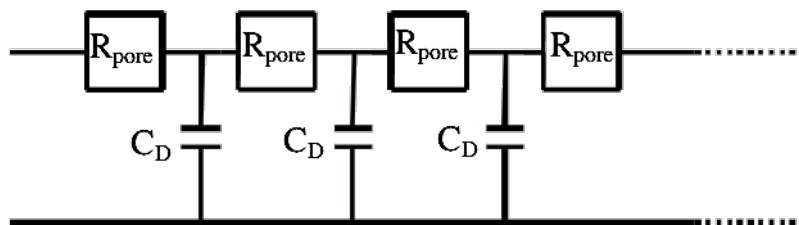
Figure 2.7: The transmission line representing the impedance inside a pore. Figure taken from [9] and modified.

The alternating potential, *E(t)*, which enters into the pore decreases from the value at the pores opening, E_0, because of the pore resistance, according to Ohm's law. Figure 2.8 shows

8

this effect where E(t) decreases with the distance in the pore, *x*. At high frequencies the alternating potential is not able to penetrate to the bottom of the pore, but for low frequencies the signal penetrates to the bottom[9]. In such cases the total impedance is a result of the contribution of the porous part of the electrode and the flat part in the bottom of the pore.
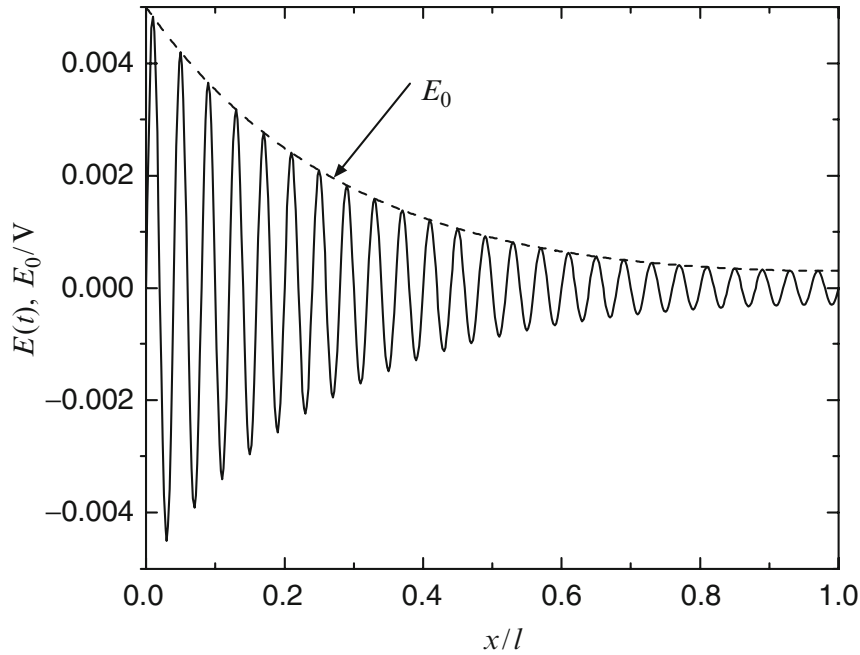
Figure 2.8: Changes of the alternating potential signal and its amplitude due to the pore depth [9].

As a general rule, the phase angle of the impedance for a porous electrode is half the phase angle for an equivalent plane electrode. In addition, the total impedance *Z* for a porous electrode is proportional to the square root of that for an equivalent plane electrode [10], as illustrated in Figure 2.9 (a) and (b).

The impedance for a porous electrode with independent pores can be written as in Eq. (2.10) [11].

$$Z_{porøs} = \sqrt{\frac{R_D}{j\omega C_D}} \, coth\sqrt{j\omega R_D C_D}$$

(2.10)

Here R_D is the resistance and C_D is the double layer capacitance.
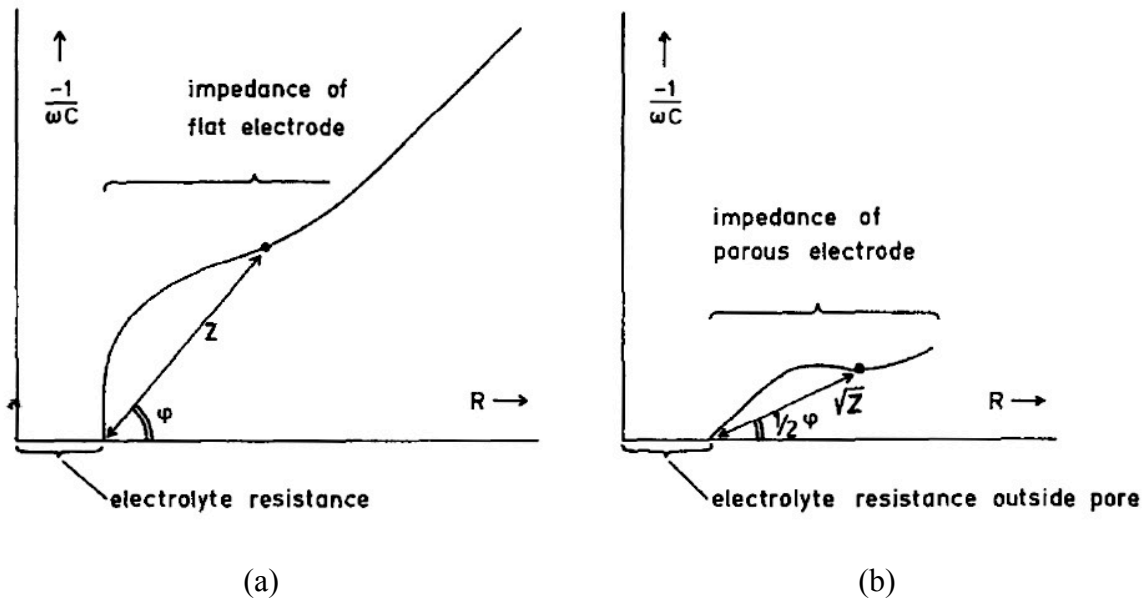
Figure 2.9: Representation of the Nyquist diagram for a planar electrode (a) and a porous electrode (b) [10].

2.1.4 Mott-Schottky behavior

When a semiconductor electrode is immersed in an electrolyte, the Fermi level of the two phases is disparate. To gain equilibrium, an exchange of charge occurs across the interface until the two Fermi levels are aligned. The band edges at the surface of the semiconductor are pinned. The charge exchange results in a bending of the energy bands in the semiconductor. This leaves a region beneath the surface depleted of charge carriers, which is called the depletion region or the space charge region. This region forms a "built-in" voltage near the semiconductors surface. The situation before and after contact is illustrated in Figure 2.10 [12]. The bands will bend differently according to the type of semiconductor. For n-type semiconductors the bands will bend upwards, as shown in (a). For p-type semiconductors the bands will bend downwards like in (b). The conductivity of most semiconductors is well below the conductivity of the solution, which means that most of the potential drop occurs in the semiconductor side of the junction [4]. Because of this, the interfacial capacitance is in most cases dominated by the capacitance due to the space charge region and the contribution from the Helmholtz layer can be neglected.

10
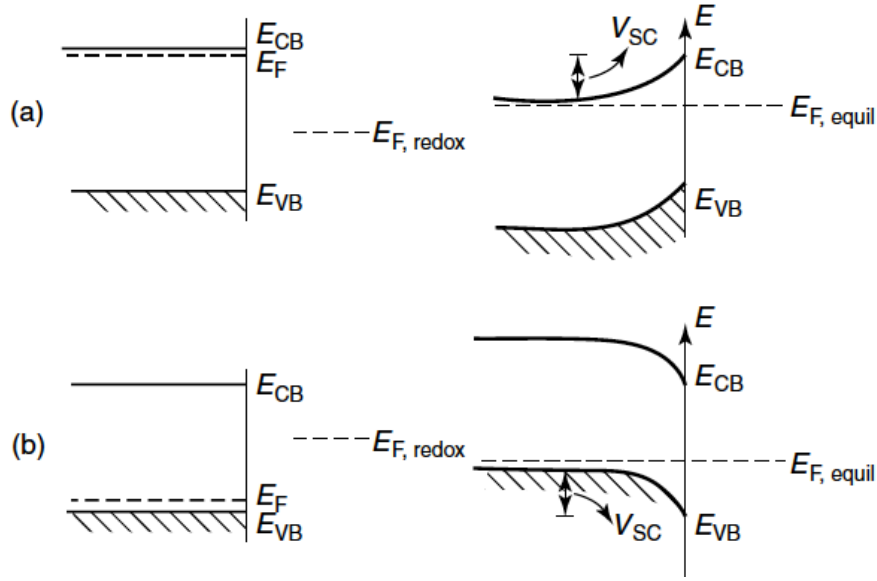
Figure 2.10: The energy bands in the semiconductor before (left) and after (right) contact with the electrolyte. For a n-type semiconductor the bands will bend upwards (a) and for a p-type semiconductor the bands will bend downwards (b) [12].

Changing the potential of the semiconductor by applying an external voltage will separate the two Fermi levels and hence influence the band bending [13]. In the case of n-type semiconductors, positive polarization will increase the band bending, while negative polarization will decrease it. If the electrode is polarized to the point where no band bending occurs, then the semiconductor is polarized to its flatband potential. This is one of the fundamental properties of semiconductors and it can be determined by using the Mott-Schottky equation, which is derived from Poisson's equation [13]:

$$\frac{d^2\phi}{dx^2} = -\frac{\rho}{\varepsilon_0 \varepsilon_s} \qquad (2.11)$$

where ϕ is the potential difference in a phase, ρ is the charge density at position x away from the semiconductor surface, ε_s is the dielectric constant of the semiconductor and ε_0 is the permittivity of free space. By applying Boltzmann distribution for the electrons in the space charge region and Gauss' law relating to the electric field caused by the charge contained in the region, Poisson's equation can be solved to give the Mott-Schottky equation [13]. For a n-type semiconductor the Mott-Schottky equation is expressed as in Eq. (2.12)[4]. A complete derivation is shown in the Supplemental Material of Ref. [13].

$$\frac{1}{C_{SC}^2} = \frac{2}{eN_D\varepsilon_0\varepsilon_s}[(E - E_{fb}) - \frac{k_BT}{e}]$$ (2.12)

Here C_{SC} is the interfacial capacitance, N_D is the concentration of donors, T is the temperature, k_B is the Boltzmann's constant and e is the electronic charge. E is the applied voltage and E_{fb} is the flatband potential. As seen from Eq. (2.12), the Mott Schottky plot of $1/C_{SC}^2$ as a function of the potential, E, should yield a straight line with a positive slope for n-type semiconductor. For a p-type semiconductor the slope will be negative. The donor and acceptor densities can be calculated from the slope and the flatband potential can be determined by extrapolating the straight line to intersect with the abscissa, as shown in Figure 2.11.
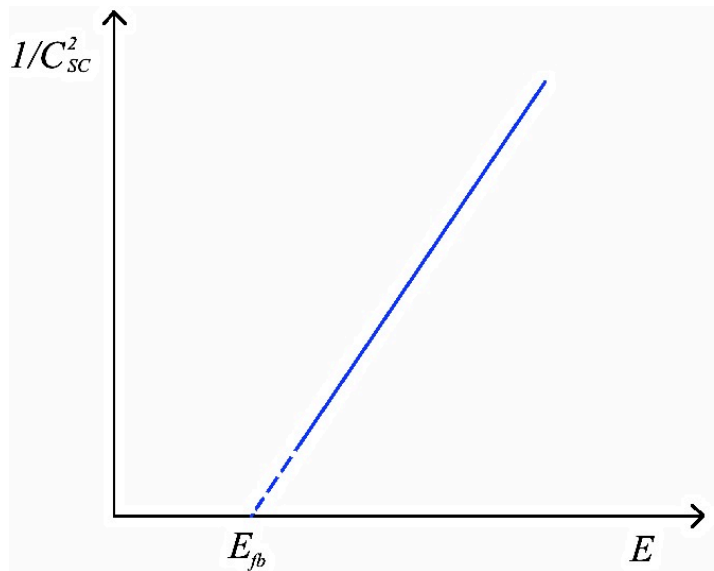
Figure 2.11: Sketch of the Mott-Schottky diagram for n-type semiconductor. The flatband potential, E_{fb}, can be found by extrapolating the straight line to intersect with the abscissa.

2.1.5 Photo-electrochemical characterization

When a semiconductor is radiated by light, electrons may be excited from the valence band to the conduction band, which leaves a hole in the former band. The generated electron-hole pairs, is separated by the electric field generated in the space charge region. Generation of electron-hole pairs requires photons energy higher than the semiconductors band gap, E_g. The relationship between the photon energy, E_{ph}, and the wavelength, λ, is given by the Planck relationship [14],

$$E_{ph}(\lambda) = \frac{hc}{\lambda}$$

(2.13)

where h is Planck's constant and c is the speed of light. When a semiconductor in an electrochemical cell is illuminated, excess charge carriers are generated that increases the current flowing through the cell. This current can be detected during photo-electrochemical measurements.

2.2 Mathematical tools

The impedance model presented in the next chapter is based on the use of the Green's function. A short introduction of this and some other tools involved is given in this chapter.

2.2.1 The δ-function

The δ-function is not strictly speaking a function, but is often thought of as an extremely narrow distribution. As an example it can be used to describe pulses of "infinitely short" duration, like strongly peaked currents that often occur during switching processes in electrical circuits. Symbolically the δ-function can be given as[15]

$$\delta(x) = \begin{cases} 0 & (x \neq 0) \\ \infty & (x = 0) \end{cases}$$

(2.14)

and this is normalized so that[15]

$$\int_{-\infty}^{+\infty} \delta(x)\, dx = 1$$

(2.15)

The δ-function can be used in combination with a continuous function $f(x)$ to give the integral [15]

$$\int_{-\infty}^{+\infty} \delta(x)\, f(x)\, dx$$

(2.16)

and because $\delta(x)$ is zero for all $x \neq 0$ the integration limits may be changed to $+\epsilon$ and $-\epsilon$, where ϵ is a small positive number. Because $f(x)$ is continuous at $x = 0$, its value within the interval $+\epsilon$ to $-\epsilon$ will be close to the value of $f(0)$ and one can claim that [15]

13

$$\int_{-\infty}^{+\infty} \delta(x) f(x) \, dx = \int_{-\epsilon}^{+\epsilon} \delta(x) f(x) \, dx \cong f(0) \int_{-\epsilon}^{+\epsilon} \delta(x) \, dx \qquad (\,2.17\,)$$

The approximation improves as ϵ approaches zero and it appears that by letting $\epsilon \to 0$ one has exactly [15]

$$\int_{-\infty}^{+\infty} \delta(x) f(x) \, dx = f(0) \qquad (\,2.18\,)$$

and the integrals limits $-\infty$ and $+\infty$ may be replaced by any two numbers a and b, provided that $a < 0 < b$. The integral in Eq. (2.18) is one of the useful features of the δ-function called the sifting property, where $\delta(x)$ act as a sieve. It makes it possible to select from all possible values of $f(x)$ its values at the point $x = 0$.

2.2.2   The Heaviside step function

The Heaviside function is a discontinuous function defined as [16]

$$H(x) = \begin{cases} 0 & if \ \ x < 0 \\ 1 & if \ \ x \geq 0 \end{cases} \qquad (\,2.19\,)$$

The Heaviside function, $H(x)$, approaches 0 when $x \to 0^-$, and as $x \to 0^+$ the function approaches 1.

2.2.3   Green's function

This section will only give a brief introduction to Green's function, but a full description can be found in Ref. [15] and [17]. Green's function is generally used to solve inhomogeneous differential equations with specific boundary conditions. The easiest way to explain how the function works is to use an example considering a stretched string pinned at the points $x = 0$ and $x = L$ [15]. The problem in the example is sketched in Figure 2.12.

The displacement, $u(x)$, of the string is a function of x alone and satisfies the differential equation[15]

$$\frac{du^2}{dx^2} = \frac{F(x)}{T} = f(x) \qquad (\,2.20\,)$$

where $F(x)/T$ is the force working on the string at position x.

14
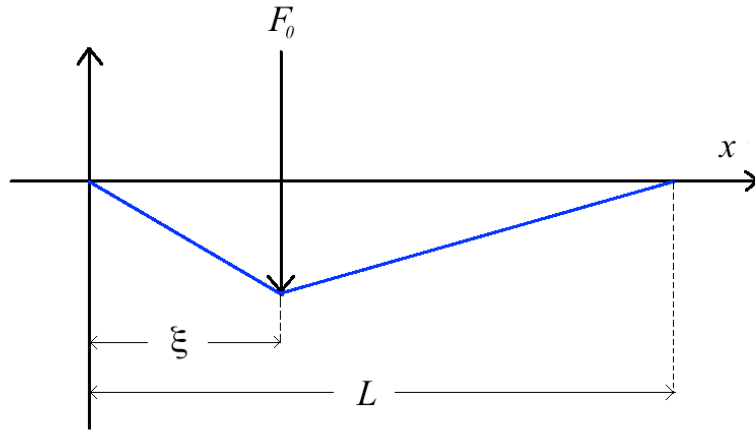
Figure 2.12: Graphical presentation of the string-problem used to explain Green's function.

By considering a concentrated load, F_0, at the point $x = \xi$ the function will be [15]

$$f(x) = \frac{F_0}{T} \delta(x - \xi) \qquad (2.21)$$

The differential equation to be solved then becomes [15]

$$\frac{dG(x|\xi)^2}{dx^2} = \delta(x - \xi) \qquad (2.22)$$

and this is now called the Green's function for the string problem. The requirements for the function is that [15]

$$G(0|\xi) = G(L|\xi) = 0 \qquad (2.23)$$

and $G(x|\xi)$ satisfies the homogenous differential equation for all x except $x = \xi$. Since $G(x|\xi)$ represents the idealized physical shape of the string, as shown in Figure 2.12, it must be continuous at $x = \xi$ and the shape will be given by [15]

$$G(x|\xi) = \begin{cases} -\dfrac{x(L - \xi)}{L}, & (0 \le x \le \xi) \\ -\dfrac{\xi(L - x)}{L}, & (\xi \le x \le L) \end{cases} \qquad (2.24)$$

The solution to the non-homogeneous problem in Eq. (2.20) with the boundary conditions in Eq. (2.23) will be given by [15]

15

$$u(x) = \int_0^L G(x|\xi) \frac{F(\xi)}{T} d\xi \qquad (\,2.25\,)$$

As a result of the shape of *u(x)* there should be a jump discontinuous in the point $x = \xi$ for
dG(x|ξ)/dx.

The Green's function is also called the influence function because is describes the response of
each point in the system to a concentrated impact, e.g. a load pulling down on a string in one
specific point.

2.3 The Impedance Model for Porous Semiconducting electrodes

The impedance model for porous semiconducting electrodes described in this section was
derived by Sunde and Tjelta and is presented in Ref. [2]. The main focus of the model is the
Mott Schottky behaviour of semiconductors.

2.3.1 The porous electrode

The system to be modelled consists of a porous film deposited on a planar substrate as
depicted in Figure 2.13. The interface between the substrate and the film is denoted $x = L$ and
the film faces the electrolyte at $x = 0$. The porous film is presented as tightly packed spherical
particles with radius R_a, in which the electrons and holes diffuse radially outside the space
charge region facing the electrolyte. In this presentation of the model it is assumed that only
electrons may reach the species in the electrolyte, because normally only one of the bands are
active in faradaic processes. Still, it is important to note that this is a general model and it can
easily be reworked to apply to holes instead of electrons [2].
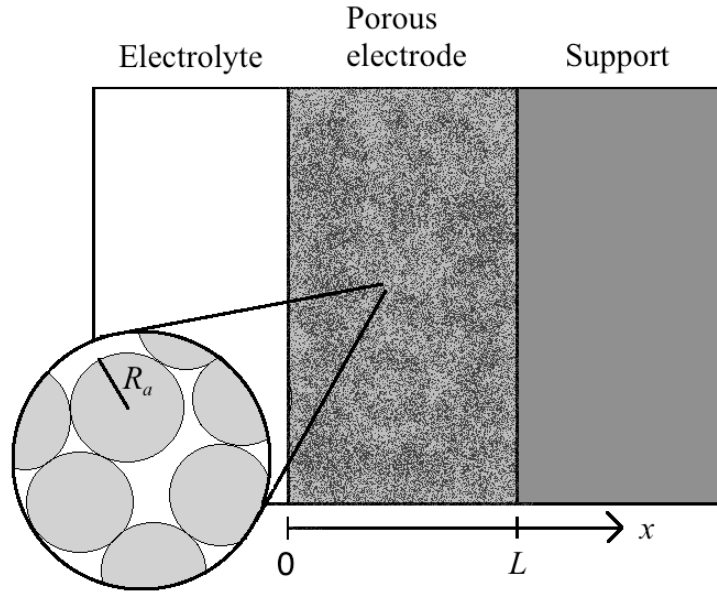
Figure 2.13: The structure of the electrode considered in the impedance model. The porous semiconductor electrode consists of small sperical particles with radius, Ra. The electrode film is in contact with the electrolyte at $x = 0$ and with the support at $x = L$. The figure is copied with modifications from [3].

The species assumed to be present in the solid phase are electrons and holes, with concentrations n and p respectively, and acceptor dopants with concentration N_A and donor dopants with concentration N_D. Assuming electroneutrality outside of the space charge region allows the use of Eq. (2.26) [2].

$$p - N_A - (n - N_D) = 0 \qquad (2.26)$$

The charge density, ρ, at a position x away from the semiconductor surface is given by [13]

$$\rho = e(p - N_A - n + N_D) \qquad (2.27)$$

where e is electronic charge.

2.3.2 The capacitance of the space charge region

To model the space charge region of the system, the Poisson-Boltzmann equation is used with assumption of spherical coordinates and spherical symmetry. This results in the following equation [2].

$$\frac{1}{r^2}\frac{d}{dr}\left(r^2\frac{d\phi}{dr}\right) - \frac{e}{\varepsilon_0\varepsilon_s}\left[n_0 - p_0 - n_0\exp\left(-\frac{e\phi}{k_BT}\right) + p_0\exp\left(\frac{e\phi}{kT}\right)\right] = 0 \tag{2.28}$$

Here r is the radius of the particles in the film, ϕ is the electrostatic potential in the space charge region, while n_0 and p_0 is the bulk concentration of electrons end holes respectively. A non-dimensional formulation of Eq. (2.28) [2] is

$$\frac{1}{x^2}\frac{d}{dx}\left(x^2\frac{du}{dx}\right) - \frac{e}{\varepsilon_0\varepsilon_s}\left[N_0 - P_0 - N_0\exp(-u) + p_0\exp(u)\right] = 0 \tag{2.29}$$

where $u = e\phi/k_BT$ and $x = r/R_a$, while $N_0 = (R_a^2e^2n_0)/(k_BT\varepsilon_s\varepsilon_0)$ and $P_0 = (R_a^2e^2p_0)/(k_BT\varepsilon_s\varepsilon_0)$. The suitable boundary conditions in this case are [2]

$$u' = 0 \ \text{ when } \ x = 0 \tag{2.30}$$

$$u = u_s \ \text{ when } \ x = 1 \tag{2.31}$$

The general case of Eq. (2.29) is difficult to solve, and for that reason the limiting cases of heavily doped and intrinsic semiconductors are considered. In the latter case, $N_0 = P_0$, which means that Eq. (2.29) becomes [2]

$$\frac{1}{x^2}\frac{d}{dx}\left(x^2\frac{du}{dx}\right) - 2N_0 sin(u) = 0 \tag{2.32}$$

This makes it possible to approximate the solution of Eq. (2.29) by expressing the fixed-point solution as an integral and apply Picard iteration. By defining the charge density for a n-type semiconductor as [2]

$$\rho_n(x) = [N_0 - P_0 - N_0\exp(-u) + p_0\exp(u)] - k^2u \tag{2.33}$$

where k^2u is the linearized charge, Eq. (2.29) can be written as [2]

$$\frac{1}{x^2}\frac{d}{dx}\left(x^2\frac{du}{dx}\right) - k^2u = \rho_n(x) \tag{2.34}$$

Hence, by applying the theory described in Chap. 2.2.3, the Green's function, G_u, for Eq. (2.34) satisfies [2]

18

$$\frac{1}{x^2}\frac{d}{dx}\left[\frac{x^2\big(dG_u(x|\xi)\big)}{dx}\right] - k^2 G_u(x|\xi) = \frac{1}{x^2}\delta(x-\xi)$$

(2.35)

Here the δ-function is $1/r^2\,\delta\,(r - r_0)$ in radial coordinates. Further, by defining $w = ux$, Eq. (2.34) can be written as [2]

$$w'' - k^2 w = \varrho_n$$

(2.36)

where $\varrho_n = x\rho_n(x)$. Then the Green's function $G_w = G_u x$ for Eq. (2.35) correspondingly satisfies [2]

$$G_w(x|\xi)'' - k^2 G_w(x|\xi) = \frac{1}{x^2}\delta(x-\xi)$$

(2.37)

For the homogeneous boundary conditions, $G_w(0|\xi) = G_w(1|\xi) = 0,$ the solution of Eq. (2.37) may be written [2]

$$G_w(x|\xi) = \frac{\cosh k\,[x + (\xi - 1)] - \cosh k\,[x - (\xi + 1)]}{2k\xi\,\sinh k}$$
$$- \frac{H(\xi - x)\,\sinh k\,(x - \xi)}{k\xi}$$

(2.38)

$H(\xi - x)$ is the Heaviside step function defined so that $H(x) = 1$ when $x = 0$. Eq. (2.38) satisfies the homogeneous differential equation in Eq. (2.36), except at the points $x = \xi$ and the boundary conditions. The derivative of the Green's function in Eq. (2.38) is [2]

$$\frac{dG_w\,(x|\xi)}{dx} = \frac{\sinh k\,[x + (\xi - 1)] - \sinh k\,[x - (\xi + 1)]}{2\xi\,\sinh k}$$
$$+ \frac{\delta(\xi - x)\,\sinh k\,(x - \xi)}{k\xi} - \frac{H(\xi - x)\,\cosh k\,(x - \xi)}{\xi}$$

(2.39)

The solution to the non-linear Poisson-Boltzmann equation in Eq. (2.34) then becomes [2]

$$u(x) = u_s\frac{\sinh\,(kx)}{x\,\sinh\,(k)} + \frac{1}{x}\int_0^1 G_w(x|\xi)\rho_n(\xi)\xi^2\,d\xi$$

(2.40)

19

This is an exact, closed-form solution for the potential, but since the integral cannot easily be expressed analytically, Picard iterations can be applied to obtain $u(x)$. In practice is it also possible to employ successive under-relaxation to ensure convergence [2].

The capacitance, $C = dQ/d\phi$, can be defined in dimensionless terms as [2]

$$\chi = \frac{k_B T}{e}\frac{dQ}{d\phi} = \frac{dZ}{du} = \frac{dZ}{dx}\frac{dx}{du} = \frac{dZ}{dx}\left(\frac{du}{dx}\right)^{-1}$$

(2.41)

where Q is the total charge and $Z = Q/\phi = 4\pi \int_0^x \rho(\xi)\xi^2\, d\xi$ is the total, dimensionless charge inside a spherical shell at radius x. The derivative of the charge Z becomes [2]

$$\frac{dZ}{dx} = 4\pi\frac{d}{dx}\int_0^x \rho(\xi)\xi^2\, d\xi = 4\pi\rho(x)x^2$$

(2.42)

and derivation of Eq. (2.40) gives [2]

$$\frac{du(x)}{dx} = u_s\frac{xk\,\cosh\,(kx) - \sinh(kx)}{x^2\,\sinh\,(k)} - \frac{1}{x^2}\int_0^1 [G_w(x|\xi)\rho_n(\xi)]\xi^2\, d\xi$$
$$+ \frac{1}{x}\int_0^1 \left[\frac{dG_w(x|\xi)}{dx}\rho_n(\xi)\right]\xi^2\, d\xi$$

(2.43)

Here ρ is a function of u. The solutions from Eq. (2.42) and Eq. (2.43) can be substituted into Eq. (2.41) to calculate the dimensionless capacitance, χ.

3 Experimental

3.1 The electrochemical cell

During the electrochemical experiments a three-electrode set up was used, consisting of a working electrode (WE), counter electrode (CE) and reference electrode (REF). Figure 3.1 shows a sketch of the electrochemical cell. The sketch also shows the gas bubbler used for oxygen removal.
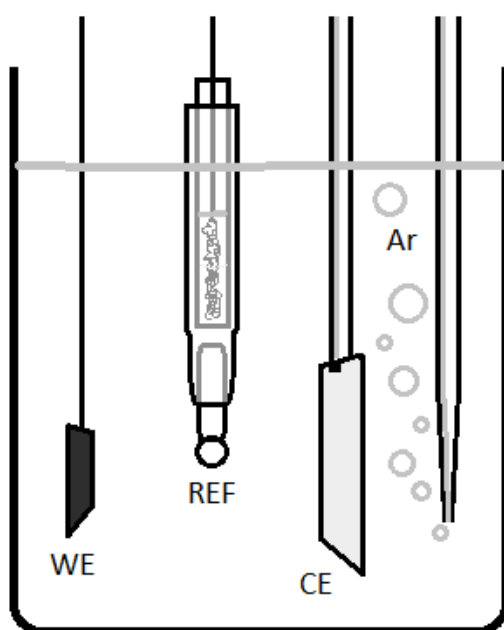
Figure 3.1: The electrochemical cell. WE is the working electrode, REF is the standard hydrogen reference electrode and CE is the Pt-foil used as a counter electrode. The electrolyte was purged with Ar-gas.

3.2 The working electrode

Three different materials were used as support for the working electrode; gold, titanium and indium tin oxides (ITO). The gold electrodes consisted of a square gold foil with a gold wire attached as a contact. The titanium electrodes were made from a 2 mm thick titanium plate. For some of the Ti-electrodes, a titanium wire was spot welded onto a square plate. Others were designed as squares with a neck that could be used as a contact. The ITO-electrodes consisted of a Pyrex™ glass plate with a thin layer of ITO on one side.

3.2.1 Pretreatment of the support material

The working electrodes were cleaned before the powder was applied. The cleaning procedures for the different materials are described in Table 3.1.

Table 3.1: Cleaning procedures for the support material before application of the powder film.

Substrate	Cleaning procedures
Au- foil	The electrode was first placed in an ultrasonic bath for 10 minutes in acetone and then etched in aqua regis (1 part HNO_3 and 3 parts HCl) for 10 seconds. After etching it was thoroughly rinsed in distilled water and dried in air.
Ti- plate	The electrode was first abraded by hand using 500 grit SiC-paper, then placed in an ultrasonic bath with acetone for 10 min. Afterwards the electrode was etched for 10 min in warm 10 wt% HCl, then rinsed in boiling distilled water for 10 min. For each step, the electrode was cooled to room temperature in the current bath before switching it to the next bath. The rinsing sequence was repeated five times. After cleaning, the Ti-supports were stored in distilled water in an attempt to limit oxidation.
ITO	The ITO glass electrode was cleaned with acetone and dried in air.

3.2.2 The oxide catalysts

Three different oxide powders were used in the experimental work. The titanium oxide powder, Aeroxide® TiO_2 P25, was produced by Degussa AG. The iridium tin oxides, $Ir_{0.25}Sn_{0.75}O_2$ and $Ir_{0.4}Sn_{0.6}O_2$, were synthesized during a previous project [18] using the polyol method.

3.2.3 Electrode preparation

The powder was applied to the support in the form of ink. The ink was made by dispersing powder in approximately 3 mL isopropanol. In some cases Nafion® was used as a binder to enhance adhesion. The mixing ratio in these cases were 95 wt% catalyst and 5wt% Nafion®. Isopropanol was then added to make a total volume of 3ml. In one case the Nafion® was dripped onto the powder film after spraying to help protect the film.

An airbrush was used to spray the catalyst ink into the support by hand. Before spraying, the ink was treated in an ultrasonic bath for 15 min to ensure dissolution of agglomerates. The support was placed on a hotplate and heated to 85° C. This heat treatment was continued through the entire spraying sequence. The spraying was started by slowly spraying the entire surface, before pausing a second to let the isopropanol evaporate. Then a new of batch ink was sprayed onto the surface, followed by a new pause. This procedure was repeated until all the ink was used. When the spraying was done, the electrode was left to dry for another 15 min on the hot plate, before it was removes and cooled to room temperature. The electrode was stored in a sealed bag.

Some of the electrodes that were made without Nafion® and these were heated to 450° C for 30 min in an inert atmosphere. This was done in a Carbolite Tube Furnace - CTF 12/65/550.

Before the electrodes were used in experiments, the backside, sides and any other areas with bare support were covered by clear nail polish. This was done to reduce the risk of interference from the support material during measurements.

3.3   Anodized titanium

A Danice Supply TPS 28 potensiostat was used to grow TiO_2 film by anodizing a titanium plate. This was done in a two-electrode setup, with the Ti-plate set up as the anode and a Pt-foil set up as the cathode. 0.5M H_2SO_4 (pH = 0.38) was used as an electrolyte. A 20 V potential was applied to the cell and held until the current was stabilized, which took approximately 50-60 min.

3.4   The standard hydrogen electrode (SHE)

The standard hydrogen electrode was prepared before each experiment using a two-electrode set up in 0,5 M H_2SO_4. A Pt-foil was used as a counter electrode and the reference electrode was set up as the working electrode. A negative potential was then applied to produce hydrogen gas until the reference electrodes tube was half filled.

3.5   The counter electrode

A platinum foil was used as counter electrode in the electrochemical and photoelectrochemical measurements. The total area of the electrode was approximately 4.5 cm^2.

3.6 Chemicals

The chemicals used during the experimental work are listed in Table 3.2. The water used during the experimental work and cleaning was produced by a Milli-Q Intergal3 system from Millipore. The resistivity of the water was 18.2 MΩcm.

Table 3.2: The chemicals used in the experimental work.

Chemical	Formula	Supplier	Purity
Acetone	C_3H_6O	VWR	Technical
Argon gas	Ar	AGA	5.0
Hydrochloric acid	HCl	Merck	p.a.
Isopropanol	C_3H_8O	Arcus	Free of water and fat
Nitric acid	HNO_3	Merck	p.a.
Potassium sulfate	K_2SO_4	Alfa Aesar	ACS grade
Sulfuric acid	H_2SO_4	VWR	p.a.

3.7 Equipment and methods

All glassware was thoroughly cleaned before use in the experiments. This was done by boiling them in 10 % H_2O_2-solution for 1-2 hours, then rinsing them in distilled water several times. After the cleaning they were dried in an oven for at least 2-3 hours. Spatulas, mortars and similar equipment was washed in distilled water, dried and then wiped with acetone.

3.7.1 Electrochemical measurements

The cell was purged with Ar-gas for about 30 min before starting the electrochemical measurements. During measurements, the tube delivering Ar-gas was pulled out of the solution and placed above the surface, still supplying inert gas throughout the experiment.

Before the actual measurements, the electrode was subjected to potential cycling until the system showed a stable response. The sweep rate during the cycling was 200 mV/s and the potential limits were 0.0 V and 1.4 V. A Gamry Instruments Reference 600 potentiostat was used in most of the experiments, but for some measurements a Zahner IM6ex was used.

After the electrode was stabilized the electrochemical measurements were performed. Cyclic voltammetry was conducted between 0.0 V and 1.4 V, and the following sweep rates were

used: 5 mV/s, 10 mV/s, 20 mV/s, 50 mV/s, 100 mV/s and 200 mV/s. The step size was 0.1 mV.

The cyclic voltammetry was followed by electrochemical impedance spectroscopy. Impedance spectrums with frequency range from 100 kHz to 0.1 Hz, were recorded for 100mV intervals between 0.1 V to 1.2 V. After the impedance measurements a final cyclic voltammetry was conducted between 0.0 V and 1.6 V, with a sweep rate of 200mV/s and a step size of 2 mV. This was done to investigate the substrates interference of the measurements.

3.7.2   Photoelectrochemistry

Before and during the photoelectrochemical measurements, the cell was treated with Ar-gas as described in Chapter 3.7.1. Photo induced current was measured by irradiating the electrode using a 300W Newport xenon lamp. A 74125 Oriel Cornerstone 260 1/4m monochromator was used to generate the desired wavelength. A Zahner IM6ex potensiostat was used to control the cell voltage and record the current response.

The photocurrent was measured during constant polarization of the electrode. The current response to the applied potential was allowed to stabilize before the photoelectrochemical measurements were performed. During the actual measurements, the wavelength of the irradiating light was change from 200 nm and 700 nm, with a step size of 5 nm. The measuring time for each step was 5 seconds. Photoresponse was also measured during constant polarization of the electrode. The photoresponse was measured by irradiating the electrode for a 60 seconds interval, separated by 60 seconds "dark" interval.

3.7.3   Particle size

Particle size was measured using a Delsa™ Nano C Particle Analyzer form Beckman Coulter. The measuring cell was cleaned with distilled water before and after measurements. The last rinsing before the analysis was done by running some of the catalyst sample through the cell. The oxide catalyst was dispersed in distilled water (5mg/50ml) and treated in an ultrasonic bath for 15 min before starting the analysis. A series of three measurements was done for each sample.

4 Results

The two main focuses in this project are the experimental analysis of TiO_2 P25 and the analysis of the impedance model for porous semiconductor electrodes, described in Chapter 2.3.2. The experimental results concerning TiO_2 P25 are presented in this chapter. In addition, the results concerning iridium tin oxide electrodes are also presented here. The results form cyclic voltammetry and electrochemical impedance spectroscopy are presented in Chapter 4.2 and Chapter 4.3, respectively. Results from photoelectrochemical measurements are presented in Chapter 4.4 and Chapter 4.5 presents the particle size analysis of the oxide catalysts. During a previous project [18], the work to derive an alternative Mott-Schottky analysis for porous electrodes was started. However, the previous derivation was not correct. A corrected derivation of the relationship between the capacitance, *C*, and the imaginary part of the impedance, *ImZ*, is presented in Chapter 4.6. The results of the computer simulation of the impedance model for porous semiconductor electrodes are presented in a separate section.

4.1 Electrodes

Three different support materials were used during the experimental work. An overview of the electrodes prepared for the experimental work is given in this section. The bare support electrodes listed in Table 4.1 were subjected to the same electrochemical measurements as the catalyst electrodes. This was done to generate reference measurements to be used in the analysis of the data collected for the catalysts. Table 4.2 lists the oxide catalyst electrodes prepared and used in the experimental work. The electrode names given in column 1 are in some cases used to refer to the electrodes. The electrode area and the catalyst loading are also given in the table. For the P25 Au N-electrode a high catalyst load was used. As a result of this the film cracked as shown in Figure 4.1 (a). A lower catalyst loading was used for P25 Au Ntop and this produced a denser film without cracks, as shown in Figure 4.1 (b).

Table 4.1: Support electrodes for which electrochemical measurements were done as a reference.

Electrode support	Area (cm^2)	Description
Au	1.071	Bare gold foil with a gold wire attached as a contact.
Ti 450	0.97	Titanium plate heated in tube furnace at 450°C for 30 min.
ITO	1.91	ITO-film on glass plate.

Table 4.2: Description of the oxide catalyst electrodes used in the experimental work.

Electrode name	Area (cm^2)	Catalyst loading (mg/cm^2)	Description
P25 Au N	1.05	8.43	P25 sprayed onto Au-support as ink with Nafion®.
P25 Au Ntop	0.93	1.53	P25 sprayed onto Au-support. Nafion® was dripped onto the film after drying.
P25 Ti N	1.03	0.59	P25 sprayed onto Ti-support as ink with Nafion®.
P25 Ti 450	0.82	2.15	P25 sprayed onto Ti-support as ink, then sintered at 450°C for 30 min.
P25 ITO	2.58	0.57	P25 sprayed onto ITO-support as ink, then sintered at 450°C for 30 min.
Anodized Ti	2.07	-	Ti-plate anodized for about 50 min at a potential of 20 V.
$Ir_{0.4}Sn_{0.6}O_2$ Au	1.05	0.57	$Ir_{0.4}Sn_{0.6}O_2$ sprayed onto Au-support as ink with Nafion®.
$Ir_{0.75}Sn_{0.75}O_2$ Au	1.05	1.09	$Ir_{0.25}Sn_{0.75}O_2$ sprayed onto Au-support as ink with Nafion®.
$Ir_{0.4}Sn_{0.6}O_2$ ITO	2.63	0.55	$Ir_{0.4}Sn_{0.6}O_2$ sprayed onto ITO-support as ink with Nafion®.
$Ir_{0.25}Sn_{0.74}O_2$ ITO	4.26	0.72	$Ir_{0.25}Sn_{0.75}O_2$ sprayed onto ITO-support as ink with Nafion®.
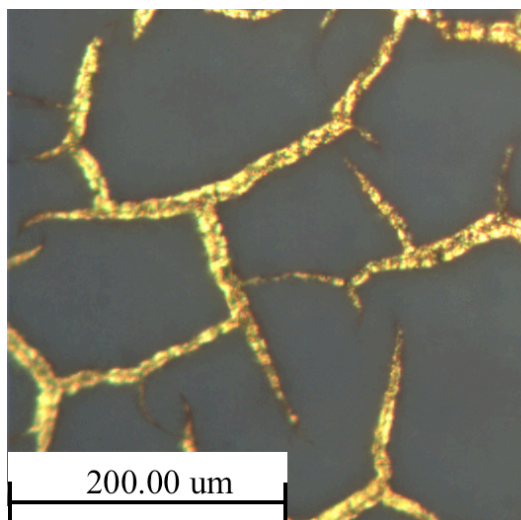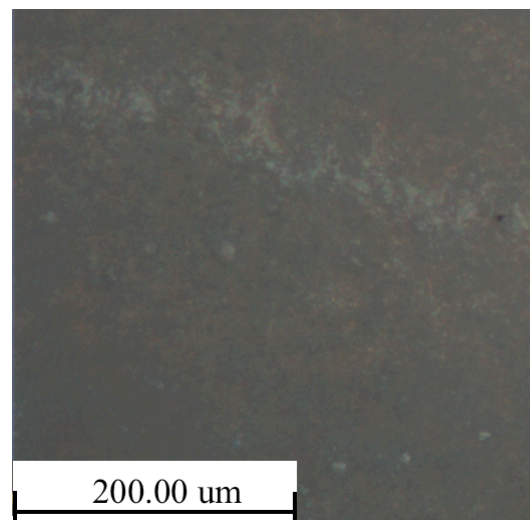
(a)   (b)

Figure 4.1: The cracked film on the P25 Au N-electrode (a) and the dense film on the P25 Au Ntop-electrode (b).

4.2 Cyclic voltammetry

4.2.1 Titanium oxide

The first substrate to be used was Au-foil. Figure 4.2 shows the voltammograms for bare Au-support (black), P25 Au N-electrode (blue) and the P25 Au Ntop-electrode (green). The sweep rate is 20 mV/s. The shape of the curves in Figure 4.2 is quite similar and only small differences can be seen. For potentials below 0.5 V the bare substrate and P25 Au N are almost identical, but for potentials above 0.5 V the P25 Au N-electrode shows somewhat larger current responses than the bare support. Above 0.5 V the measurements for bare support and P25 Au Ntop is as good as identical. This indicates that the support is dominating the measurements.

Figure 4.2: Cyclic voltammogram for the bare Au-support (black), P25 on Au-support with Nafion® mixed in the ink (blue) and P25 on Au-support, where Nafion® was dripped onto the film after drying (green). The CV was recorded on the Gamry Reference 600 potentiostat and the sweep rate is 20 mV/s.

Titanium was also tested as a support for TiO_2 P25. Figure 4.3 compares the voltammograms with sweep rates of 20 mV/s for four electrodes. For two of the electrodes, Ti was used as a support for P25, the P25 Ti N-electrode (red) and the P25 Ti 450 (green). In addition, the figure shows the voltammogram for a bare Ti-electrode also heated at 450°C for 30 min (blue) and an anodized Ti-electrode (black). For the sintered P25 and the anodized Ti-electrode peaks for oxidation and reduction are clearly visible at potentials close to zero. The

28

shape of the voltammogram for P25 Ti N-electrode bears resemblance to the Ti 450-electrode, with no oxidation peak at low voltages.

The third electrode material used in this work was ITO. The voltammogram for P25 ITO, and the bare ITO-electrode is presented in Figure 4.4. As for the other to support materials, the two bare support and P25 on ITO show great resemblance.
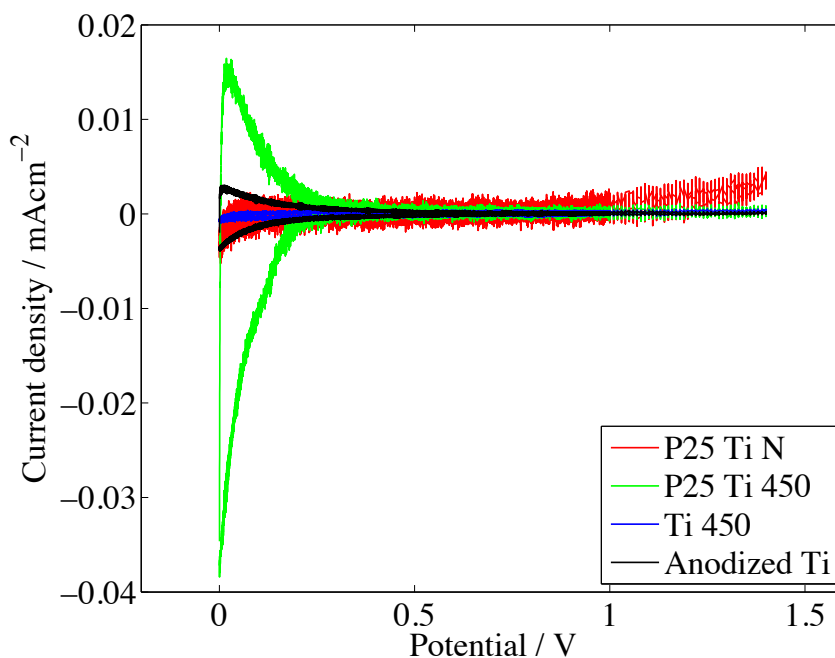
Figure 4.3: Cyclic voltammetry for Ti-supported electrodes. The P25-electrode where the ink was mixed with Nafion® (red), P25 sprayed onto the Ti-plate, then sintered at 450°C for 30 min (green) and a reference Ti-plate heated at 450°C for 30 min (blue). An anodized Ti-electrode is also represented (black). The sweep rate is 20 mV/s. (Gamry Reference 600.)
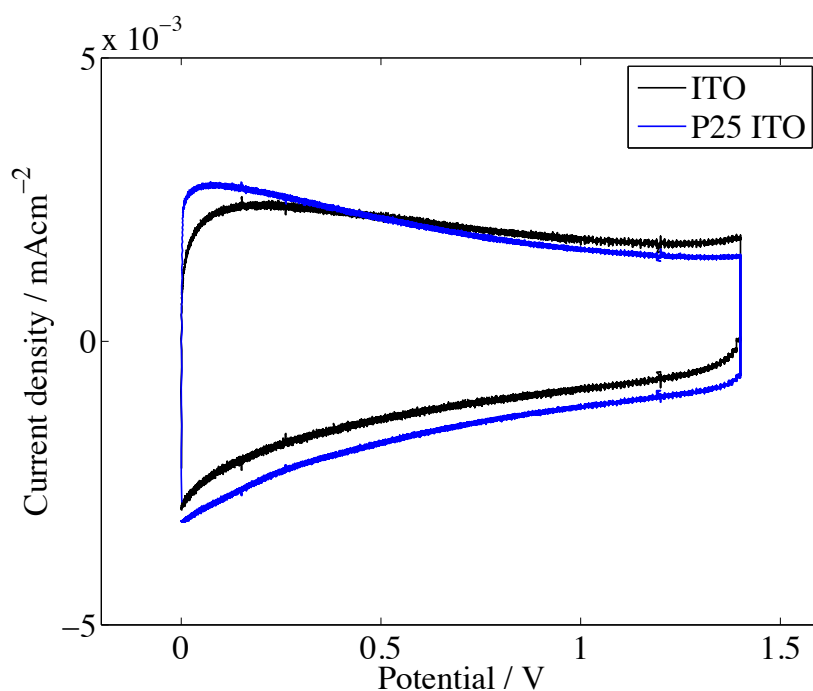
Figure 4.4: Cyclic voltammogram for P25 sprayed onto ITO, then sintered at 450°C for 30 min (blue) and bare ITO (black). The sweep rate is 200 mV/s and the Gamry Reference 600 potensiotat was used.

4.2.2 Iridium tin oxide

During the experimental work with iridium tin oxides, Au-foil and ITO was used as support. Figure 4.5 shows the voltammogram for the two support materials, recorded at a 200 mV/s sweep rate between 0.0 V and 1.6 V. The shape of the cyclic voltammogram for the ITO electrode cannot be discerned in this figure because of the scale, but the general shape can be seen in Figure 4.4. The anodic turning potential was set at 1.6 V in order to polarize the Au-electrode enough to produce the characteristic Au-peak at about 1.2 V. Figure 4.6 compares the Au-support and $Ir_{0.4}Sn_{0.6}O_2$ Au. The characteristic Au-peak can be seen in both cases.
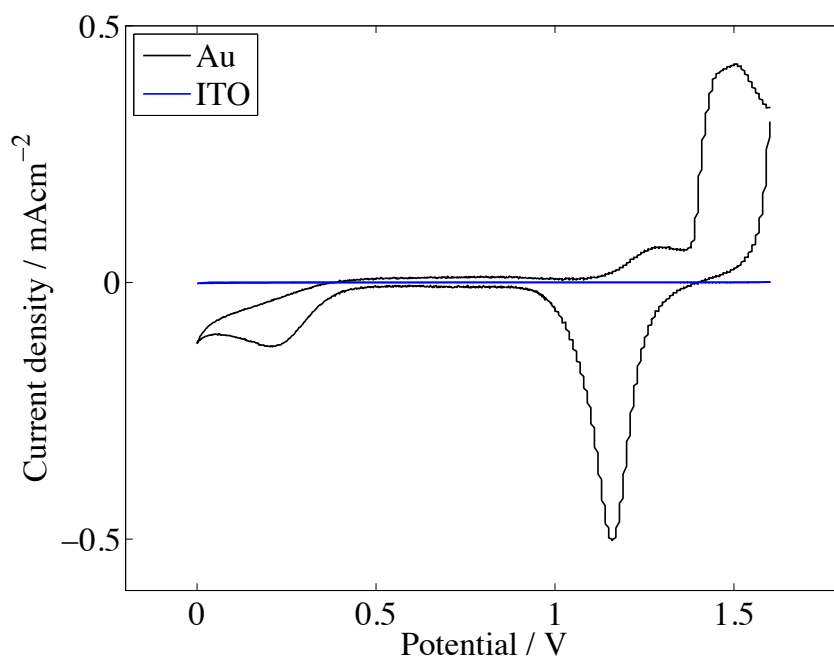
Figure 4.5: Cyclic voltammetry for the Au-support (black) and the ITO-support (blue). The sweep rate is 200 mV/s and the electrodes are cycled between 0.0 V and 1.6 V. (Gamry Reference 600)
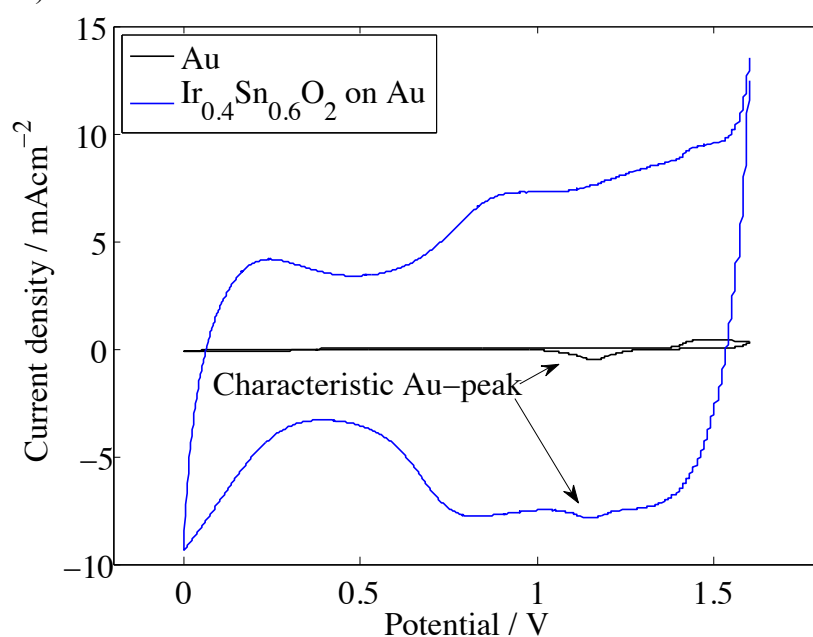
Figure 4.6: Cyclic voltammetry for bare the Au-support (black) and $Ir_{0.4}Sn_{0.6}O_2$ on Au with Nafion® (blue). The sweep rate is 200 mV/s. (Gamry Reference 600)

The cyclic voltammogram for bare ITO, the $Ir_{0.4}Sn_{0.6}O_2$ ITO-electrode and the $Ir_{0.25}Sn_{0.75}O_2$ ITO-electrode is shown in Figure 4.7. The sweep rate is 5 mV/s. The shape of the voltammogram is quite different than the shape seen for ITO in Figure 4.4.
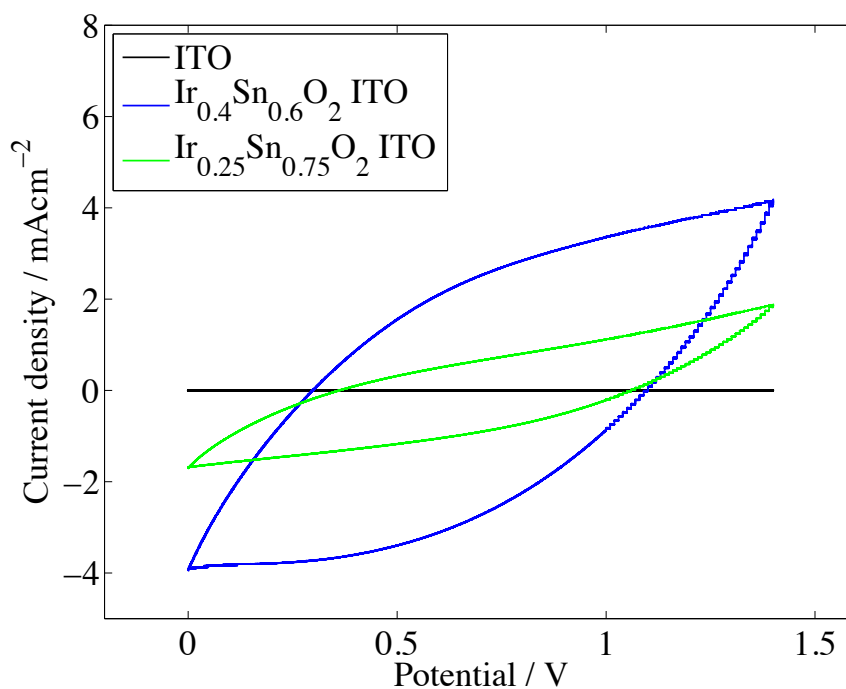
Figure 4.7: Cyclic voltammetry for bare ITO (black), $Ir_{0.4}Sn_{0.6}O_2$ ITO (blue) and $Ir_{0.25}Sn_{0.75}O_2$ ITO (green) at a sweep rate of 200 mV/s. (Gamry Reference 600)

4.3 Electrochemical impedance spectroscopy

4.3.1 Titanium oxide

The impedance measurements for P25 Au N and P25 Au Ntop also indicate that the Au-support is dominating. The difference in the logarithmic plot of the imaginary part of the impedance, ImZ, and the angular frequency, ω, is shown in Figure 4.8. The bare Au-support shows a straight line with a slope of -1. The P25 Au Ntop-electrode shows a slight curvature for low frequencies, but the slope is close to -1. The P25 Au N-electrode deviate the most from the Au-supports behavior, but it is still clearly dominated by the plane support.
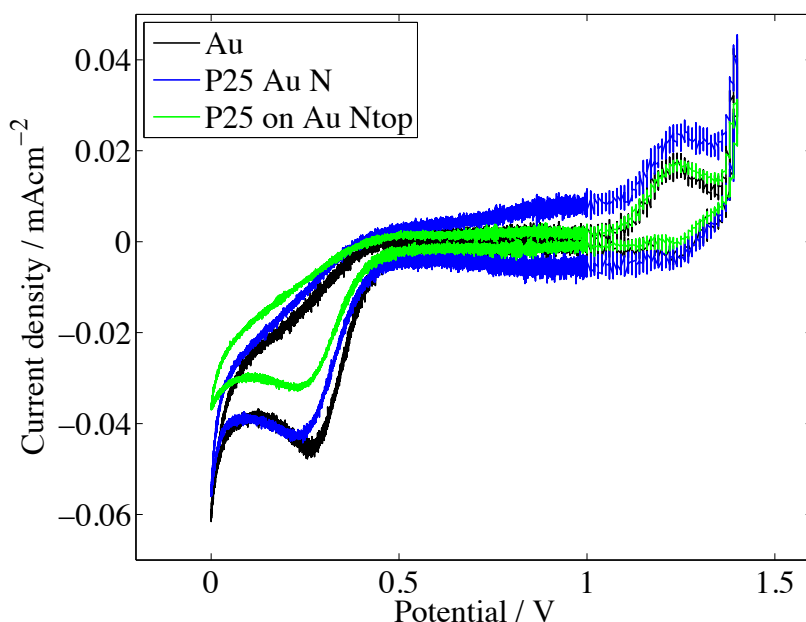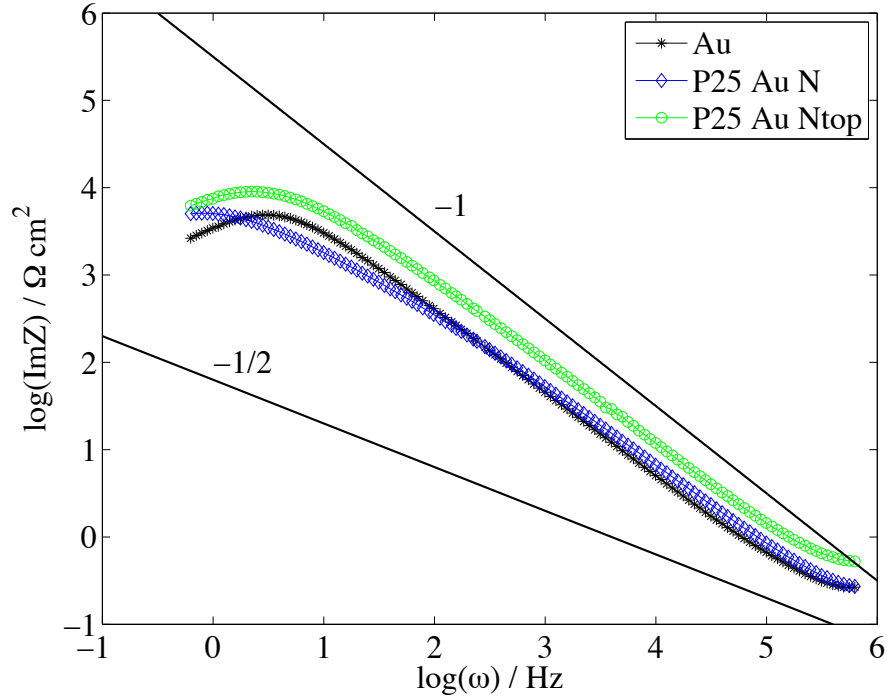
Figure 4.8: The *ImZ* vs. *ω* for bare Au-support (black), P25 on Au-support with Nafion® mixed in the ink (blue) and P25 on Au-support where Nafion® was dripped onto the film after drying (green). Measured at 400 mV using a Gamry Reference 600 potentiostat.

Also when titanium is used as a support, the impedance diagrams indicate that the measurements are dominated by the Ti-substrate. The logarithmic diagram, where *ImZ* is plotted as a function of *ω*, for the two P25-electrodes and bare Ti-support is shown in Figure 4.9. The direct potential for the graphs is 600mV. The similarities are striking and all the curves have a slope close to -1.
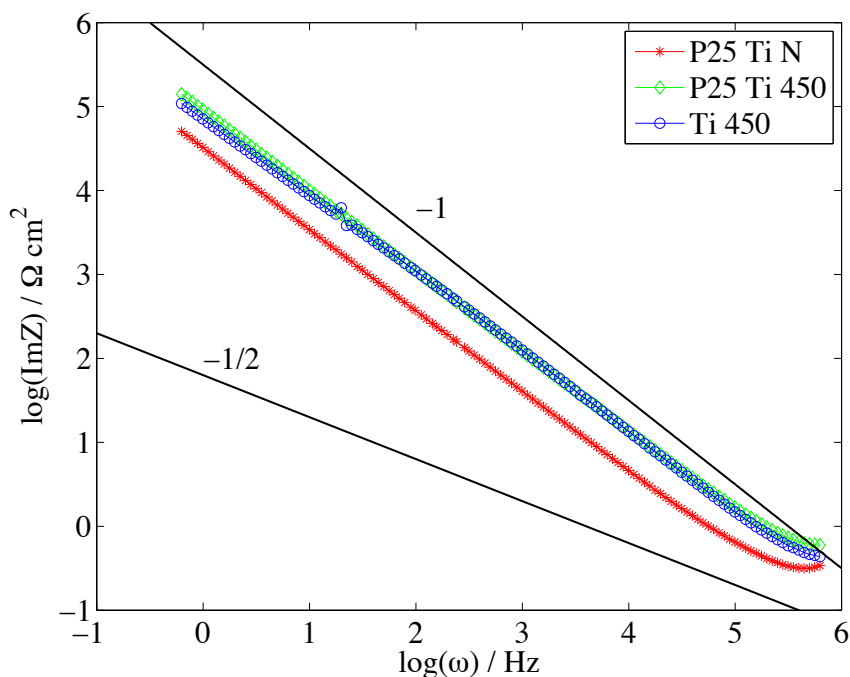
Figure 4.9: The imaginary part of the impedance vs. the angular frequency for P25 with Nafion® mixed into the ink (red), P25 sprayed without Nafion®, then sintered at 450°C (green) and bare Ti-support heat-treated at 450°C. Measured at 600 mV on a Gamry Reference 600.

However, the case is different for the anodized Ti-electrode. Figure 4.10 shows the same type of logarithmic diagram for anodized Ti, but here all the recorded spectrums are included, viz. the spectrums for all the direct potentials from 100 -1200 mV. In the low frequency part of the diagram, the slopes of the curves are slightly less than -1 and the electrode shows plane behavior. For frequencies above about 3500 Hz, the slopes for most of the curves are increased to values closer to -1/2. This indicates that the electrode shows porous behavior at high frequencies. The slopes in the low and high frequency areas were calculated as illustrated in Figure 4.11 and the results are shown in Table 4.3. As the table shows, none of the slopes in the high frequency area is exactly -1/2, but somewhat higher in negative value and increasing with increasing direct potential.
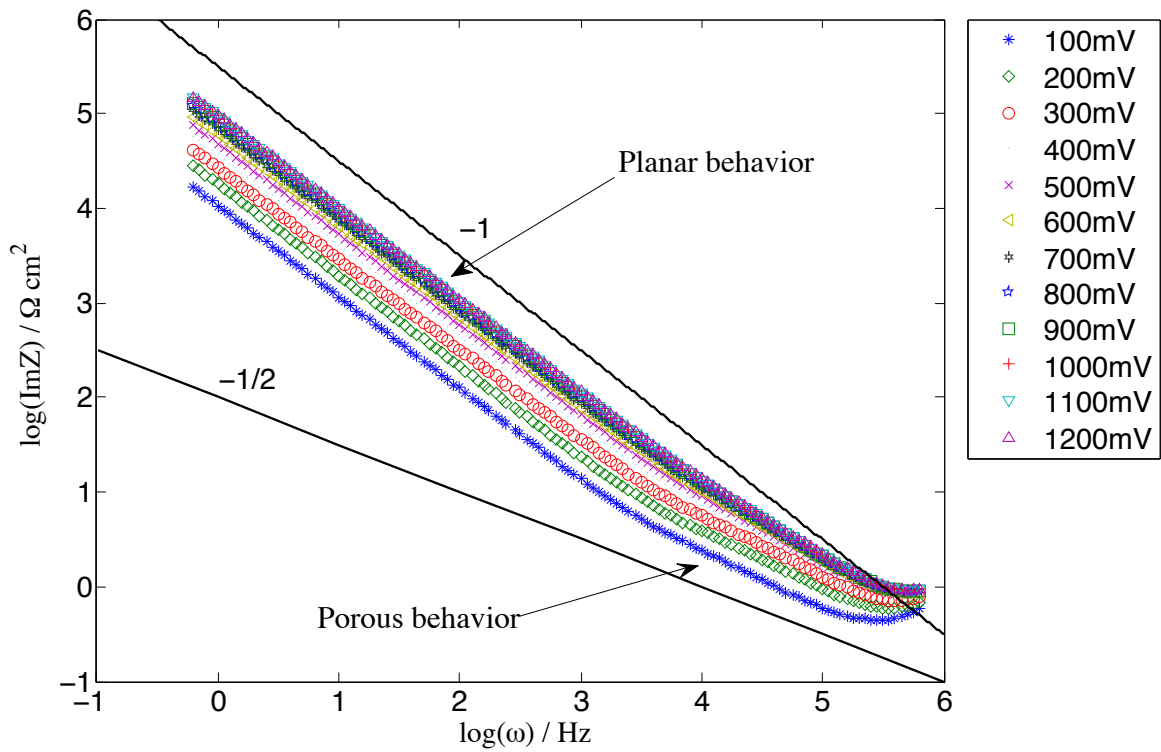
Figure 4.10: The imaginary part of the impedance vs. the angular frequency for anodized Ti. Recorded at direct potentials between 100 -1200 mV. For the high frequency part of the diagram the electrode shows porous behavior and the slopes are about -1/2. For lower frequencies the slope increases in negative value to -1. (Gamry Reference 600)
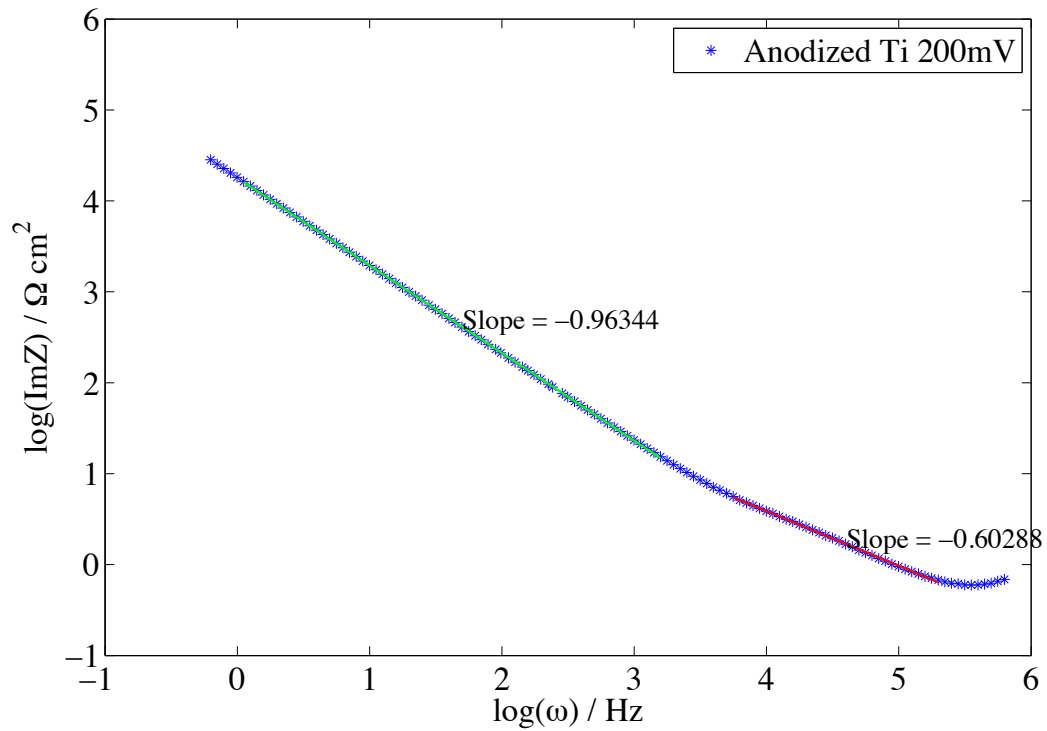
Figure 4.11: The slopes calculated for the logarithmic plot of *ImZ* vs. *ω* for anodized Ti, measured at 200 mV on a Gamry Reference 600.

Table 4.3: The slopes of the low and high frequency part of the curves in Figure 4.10. The slopes were calculated using the least squares method in MATLAB®.

Direct potential (mV)	Slope of the linear part in the low frequency area	Slope of the linear part in the high frequency area
100	-0.965	-0.598
200	-0.963	-0.603
300	-0.955	-0.629
400	-0.953	-0.677
500	-0.955	-0.698
600	-0.961	-0.735
700	-0.966	-0.749
800	-0.969	-0.760
900	-0.970	-0.776
1000	-0.971	-0.770
1100	-0.972	-0.776
1200	-0.973	-0.776

The porous behavior of anodized Ti can also be seen in the high frequency part of the Nyquist diagrams shown in Figure 4.12. The diagram for Ti 450 (a) shows near vertical lines, while the diagram for anodized Ti shows deceased phase angels. This indicates that the TiO_2-film produced by anodizing Ti is porous.

(a) (b)
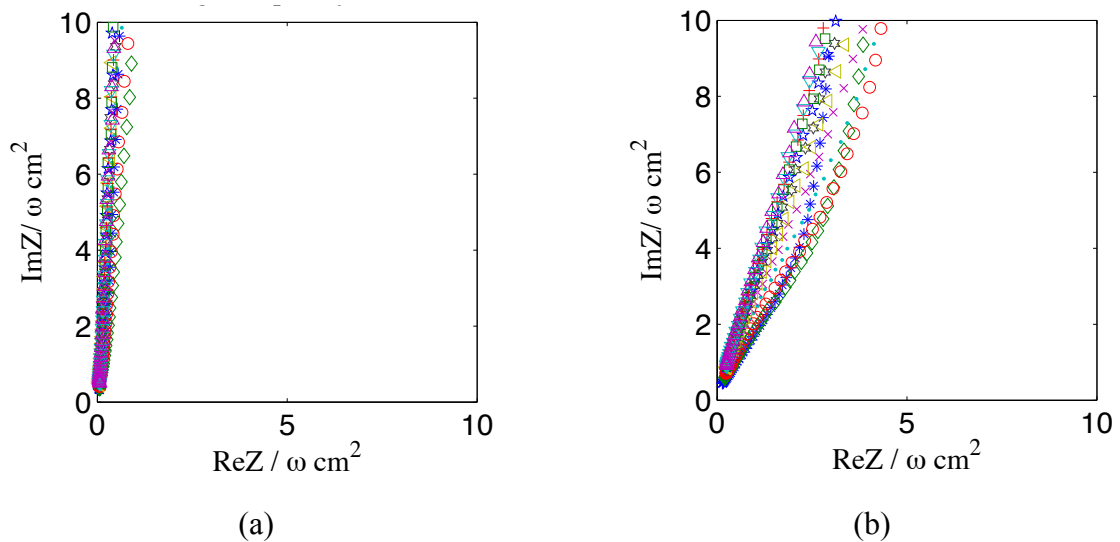
Figure 4.12: Nyquist diagram from the high frequency part for bare Ti heated at 450°C for 30 min (a) and anodized Ti (b). (Gamry Reference 600)

For the sintered P25 ITO the impedance measurements show only hints of a porous structure. The logarithmic plot of *ImZ* vs. ω is presented in Figure 4.13. This shows a small area in the

high frequency area for P25 ITO with a slope close to -1/2. This occurs at frequencies between about 8 kHz and 70 kHz. The Mott-Schottky diagrams for the two electrodes, also shows quite similar behavior, as seen in Figure 4.14.
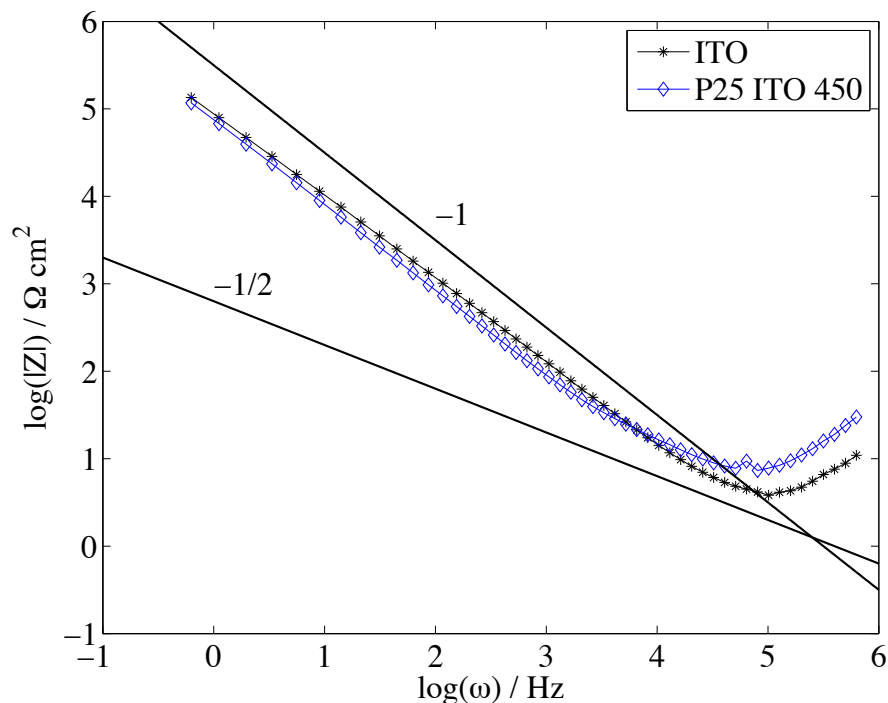
Figure 4.13: *ImZ* as a function of *ω* for P25 sprayed onto ITO, then sintered at 450°C for 30 min (blue) and bare ITO (black). Measured at a direct potential of 200 mV using a Zahner IMe6 potensiostat.
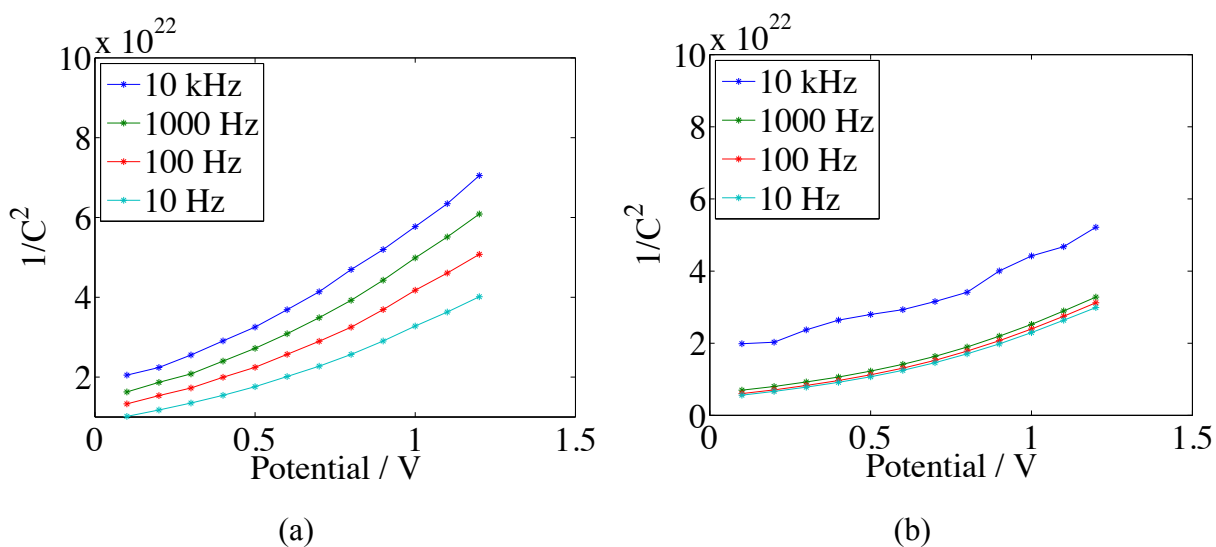
Figure 4.14: Mott-Schottky diagram for ITO-support (a) and P25 ITO (b).

4.3.2 Iridium tin oxides

Some of the impedance measurements for $Ir_{0.4}Sn_{0.6}O_2$ on Au-support give the impression that the electrode has a porous structure. The Nyquist diagram for $Ir_{0.4}Sn_{0.6}O_2$ on Au-support with Nafion® is shown in Figure 4.15. The diagram shows the curves for direct potentials between 100 - 1200 mV and the phase angle in the high frequency area is 45°. The logarithmic plot of *ImZ* as a function of ω is shown in Figure 4.16. The direct potential is 500 mV and the slope is close to -1/2 for large areas of the high frequency part.
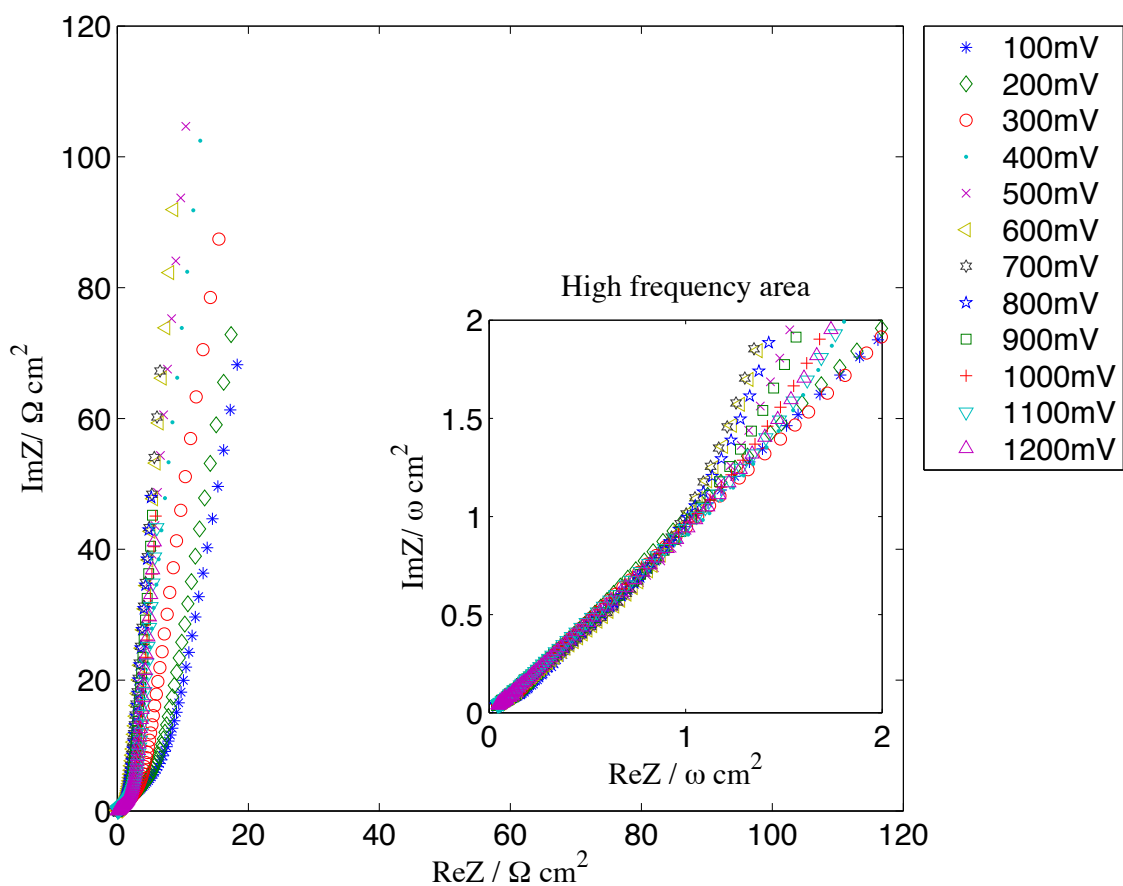
Figure 4.15: Nyquist diagram for $Ir_{0.4}Sn_{0.6}O_2$ Au. (Gamry Reference 600)
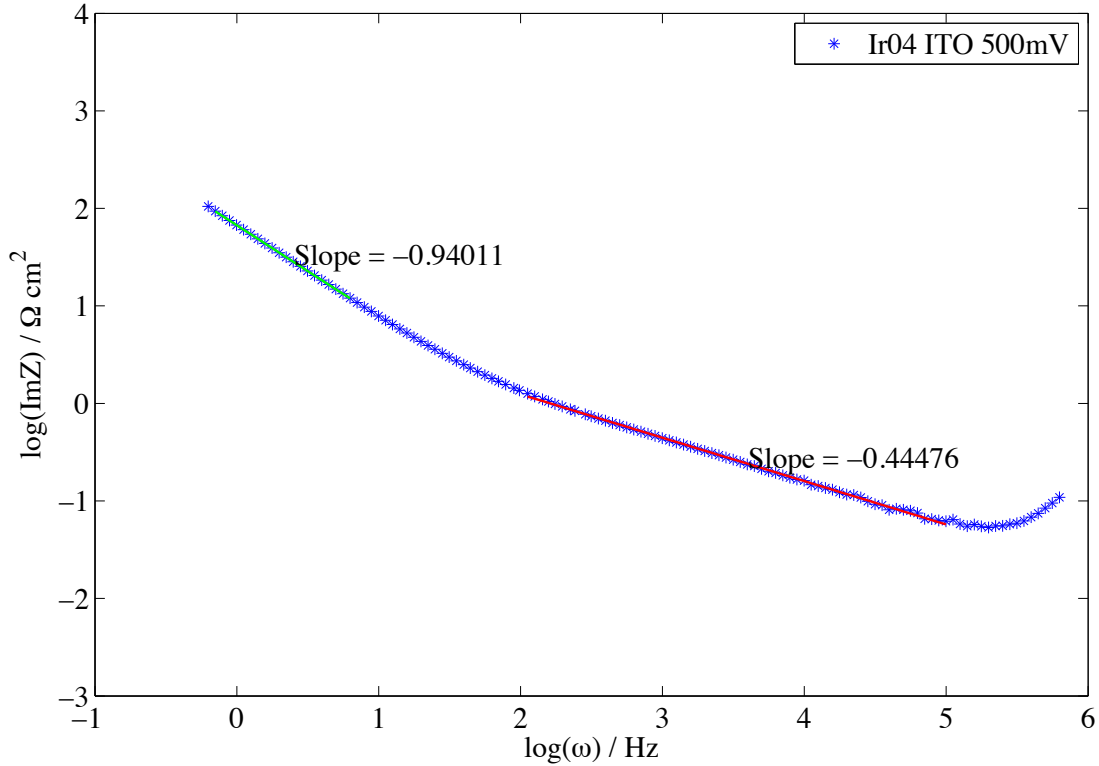
Figure 4.16: Logarithmic plot of *ImZ* and ω for $Ir_{0.4}Sn_{0.6}O_2$ on ITO-support with Nafion®. Measured at a direct potential of 500 mV. (Gamry Reference 600)

However, the Mott Schottky diagrams for the bare Au-substrate and the Au-supported $Ir_{0.4}Sn_{0.6}O_2$-electrode shows that the difference between the two electrodes are small. The Mott-Schottky diagrams for 100 kHz, 10 kHz and 1000 Hz for the two electrodes are shown in Figure 4.2. The figures to the left are the diagrams for the $Ir_{0.4}Sn_{0.6}O_2$-electrode and the diagrams for bare Au-support are shown to the right.

The impedance measurements for the $Ir_{0.25}Sn_{0.75}O_2$ Au-electrode, shows quite abnormal behavior and are therefore considered unsuccessful.

Mott-Schottky diagrams for ITO-support and $Ir_{0.4}Sn_{0.6}O_2$ ITO are shown in Figure 4.18. In this case the difference is apparent for the two electrodes, as the slope of the graphs representing the ITO-electrode is positive for all the frequencies, while the slope is negative for $Ir_{0.4}Sn_{0.6}O_2$ ITO at 1000 Hz and 100 Hz. However, as for the $Ir_{0.25}Sn_{0.75}O_2$ oxide some of the other impedance data were inconclusive.

39
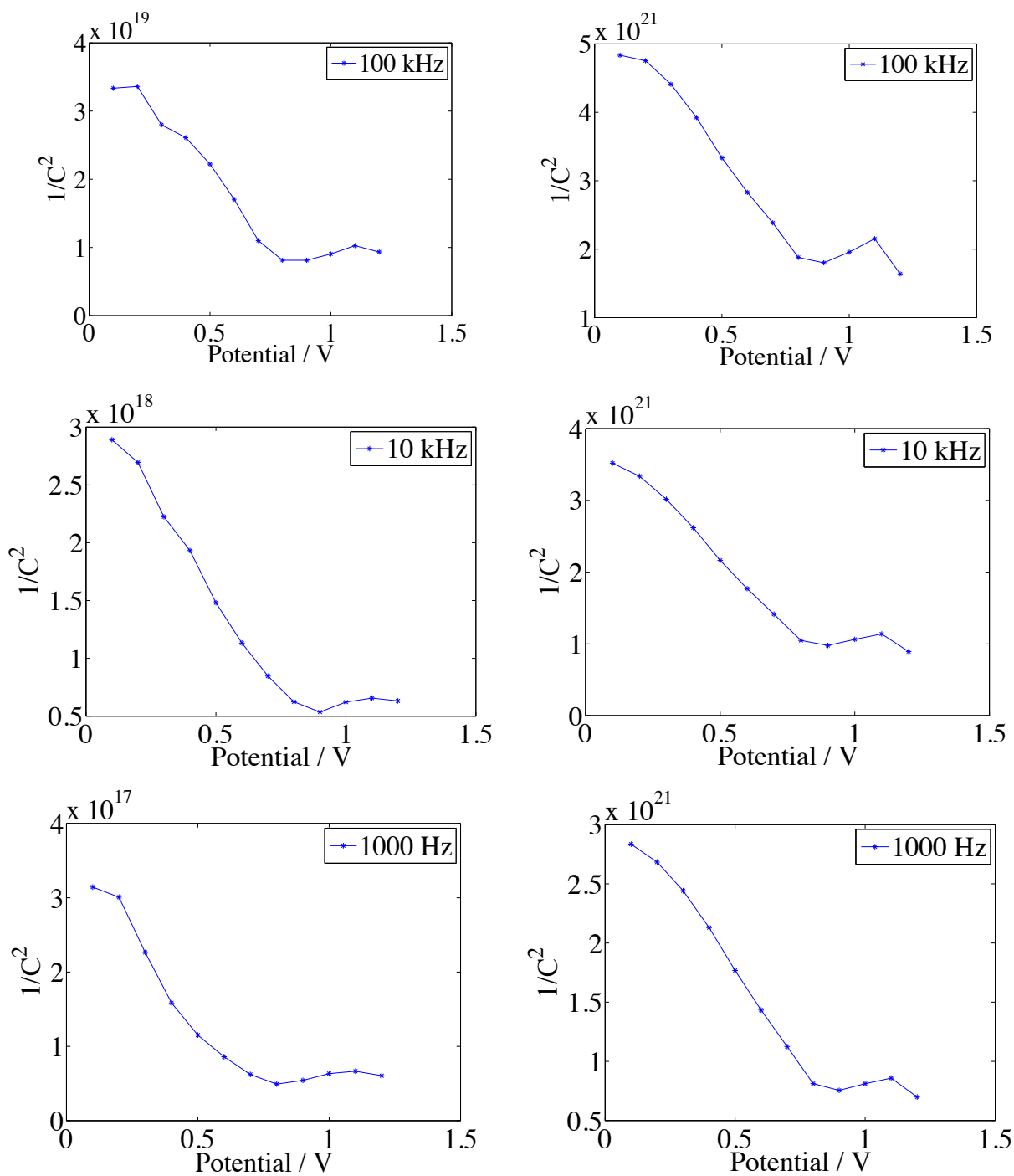
Figure 4.17: Mott-Schottky diagrams for Au (left) and $Ir_{0.4}Sn_{0.6}O_2$ Au (right), at 100 kHz, 10 kHz and 1000 Hz. Calculated from data recorded with the Gamry Reference 600.
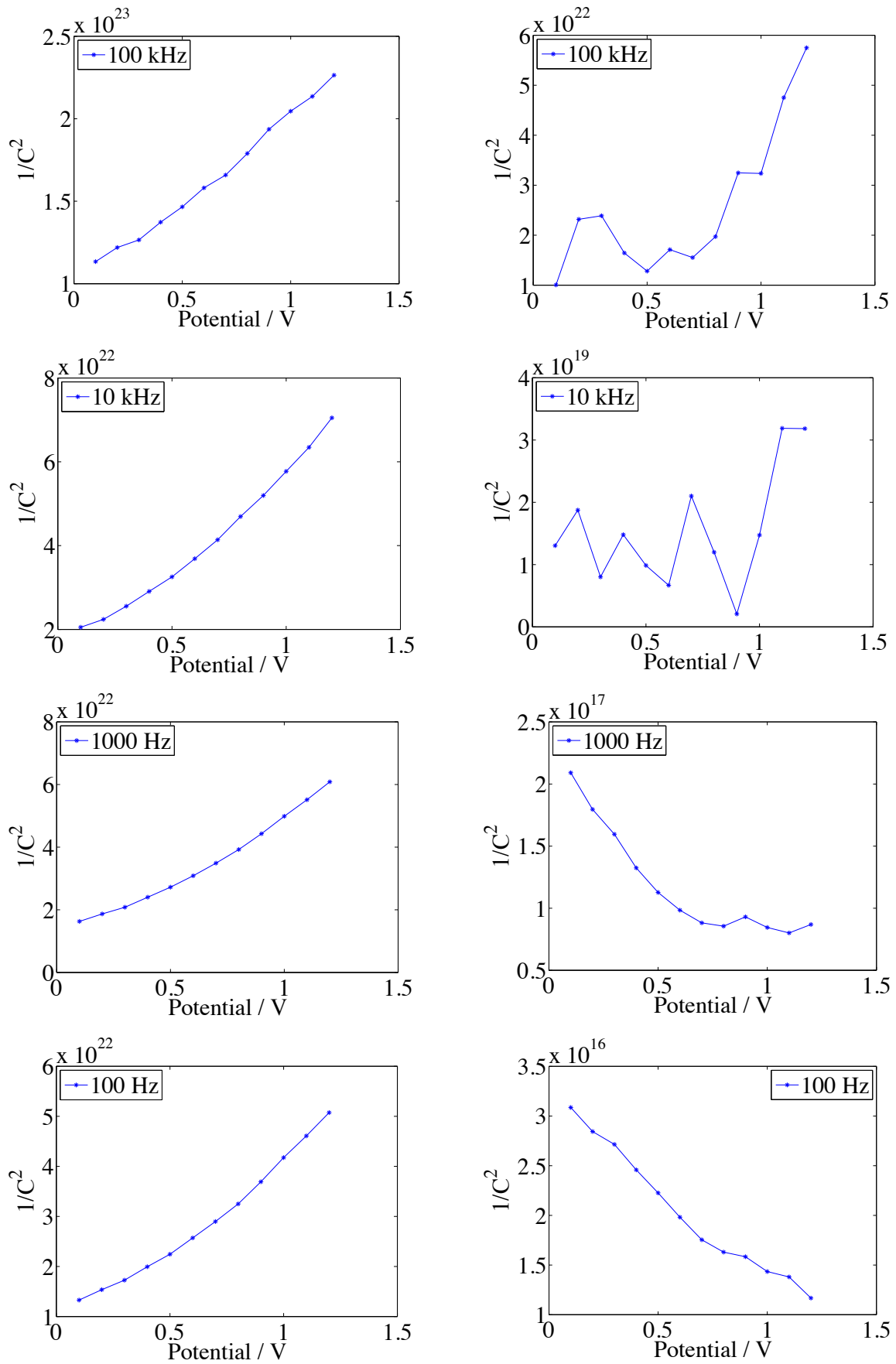
Figure 4.18: Mott Schottky diagrams for ITO-support (left) and $Ir_{0.4}Sn_{0.6}O_2$ ITO-support (right). Calculated from data recorded with the Gamry Reference 600.

4.4 Photoelectrochemisty

Photoelectrochemical measurements were performed on the sintered P25 and $Ir_{0.4}Sn_{0.6}O_2$ with Nafion®, both on ITO-support. The same measurements were also performed on bare ITO-support. Figure 4.19 shows the recorded photocurrent as a function of the lights wavelength after the background noise is removed. For bare ITO, the current peaks at a wavelength of about 310 nm, which corresponds to an optical bandgap of $E_g = 4.0$ eV. For P25 on ITO the main peak is located at approximately 365 nm, equivalent to $E_g = 3.4$ eV, and the peak has a shoulder at about 330 nm. The peak for $Ir_{0.4}Sn_{0.6}O_2$ is more difficult to discern, but the largest currents are recorded between 360 and 460 nm.

(a)

(b)

(c)
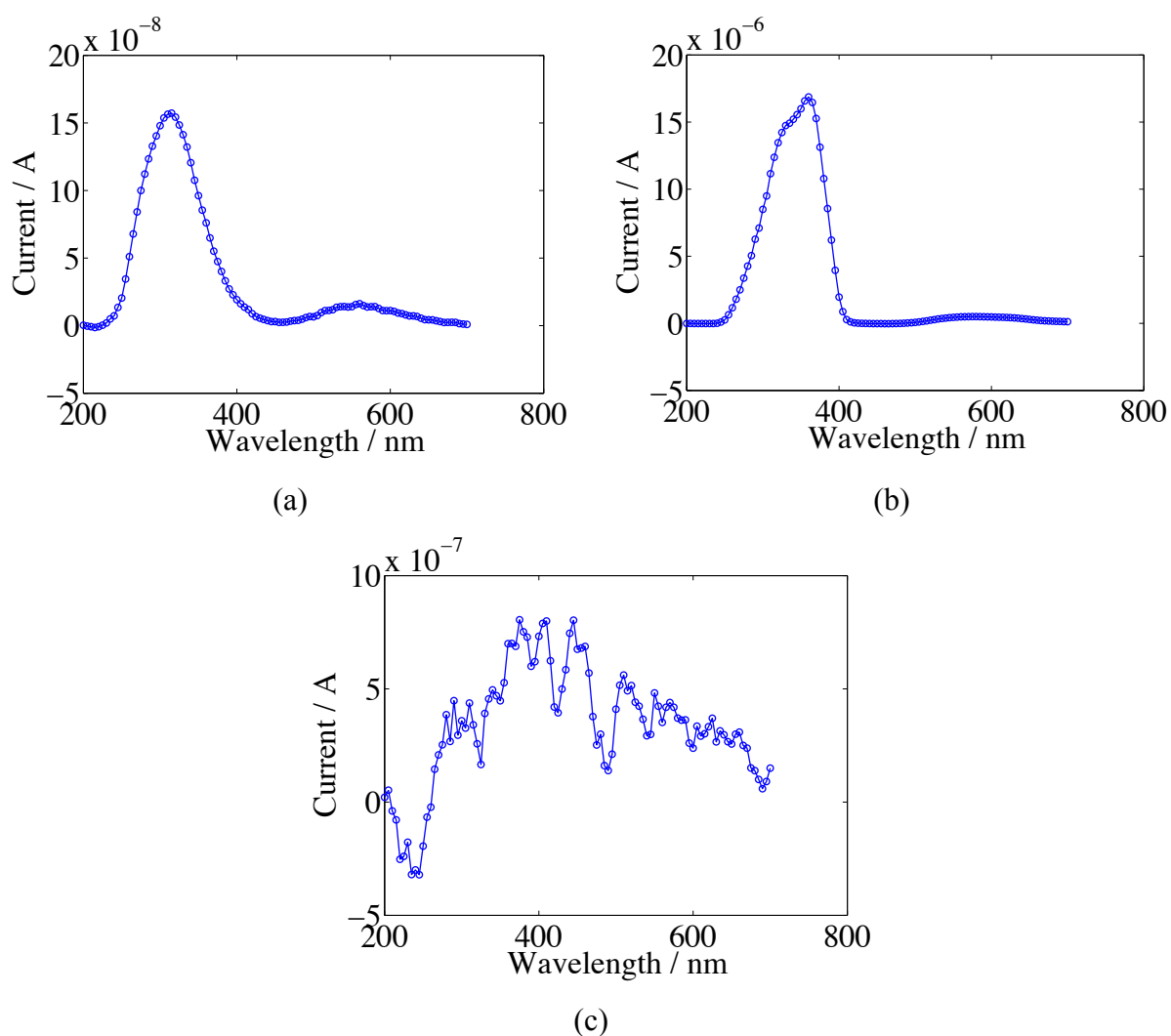
Figure 4.19: The measured current after subtraction of the background noise. The wavelength scan was performed between 200 - 700 nm, for bare ITO (a), sintered P25 on ITO (b) and $Ir_{0.4}Sn_{0.6}O_2$ (c). (Zahner IMe6)

The intensity of the light the monochromator delivers during the wavelength scan varies with the wavelength. The intensity variations are plotted in Figure 4.20, and the recorded currents in Figure 4.21 is normalized with respect to the intensity.
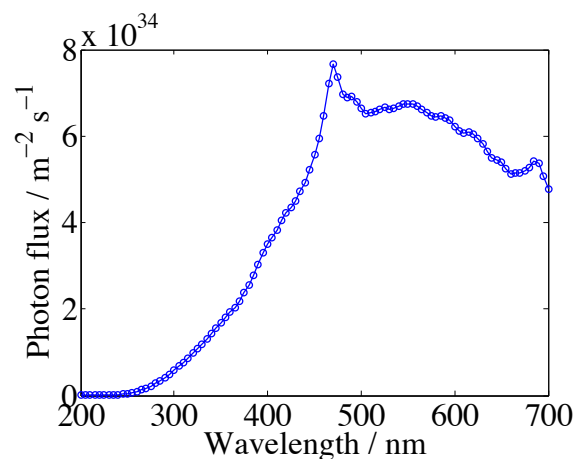
Figure 4.20: The intensity of the monochromator, here presented as photon flux as a function of wavelength.

Figure 4.21 (a) shows the normalized photocurrent for the ITO-support. The voltage generated by the potentiostat during the measurements was 1.0 V. The graph shows a peak at a wavelength of 260 nm, and the number of electrons per mol photons is about 210. For the P25-electrode, shown in Figure 4.21 (b), the main peak is shifted slightly to the right and occurs at 275 nm. This graph shows a smaller peak to the right of the main peak, at about 310 nm. It also has a shoulder starting at 360 nm. The current recorded in this case is about 28 times larger than that of the bare substrate, with 5900 electrons per mol photons. In Figure 4.21(c) the normalized current for the $Ir_{0.4}Sn_{0.6}O_2$-electrode is shown, but in this case the exact location of the main peak is harder to discern. Still, the largest current is measured at 280 nm, and it is about 2.5 times larger than the current peak measured for bare ITO.

The photoresponse for bare ITO-support and P25 on ITO was also recorded, and the results can be seen in Figure 4.22 (a) and (b), respectively. Both electrodes show a rapid response when the light is switched on and off. Photoresponse was not measured for iridium tin oxides.
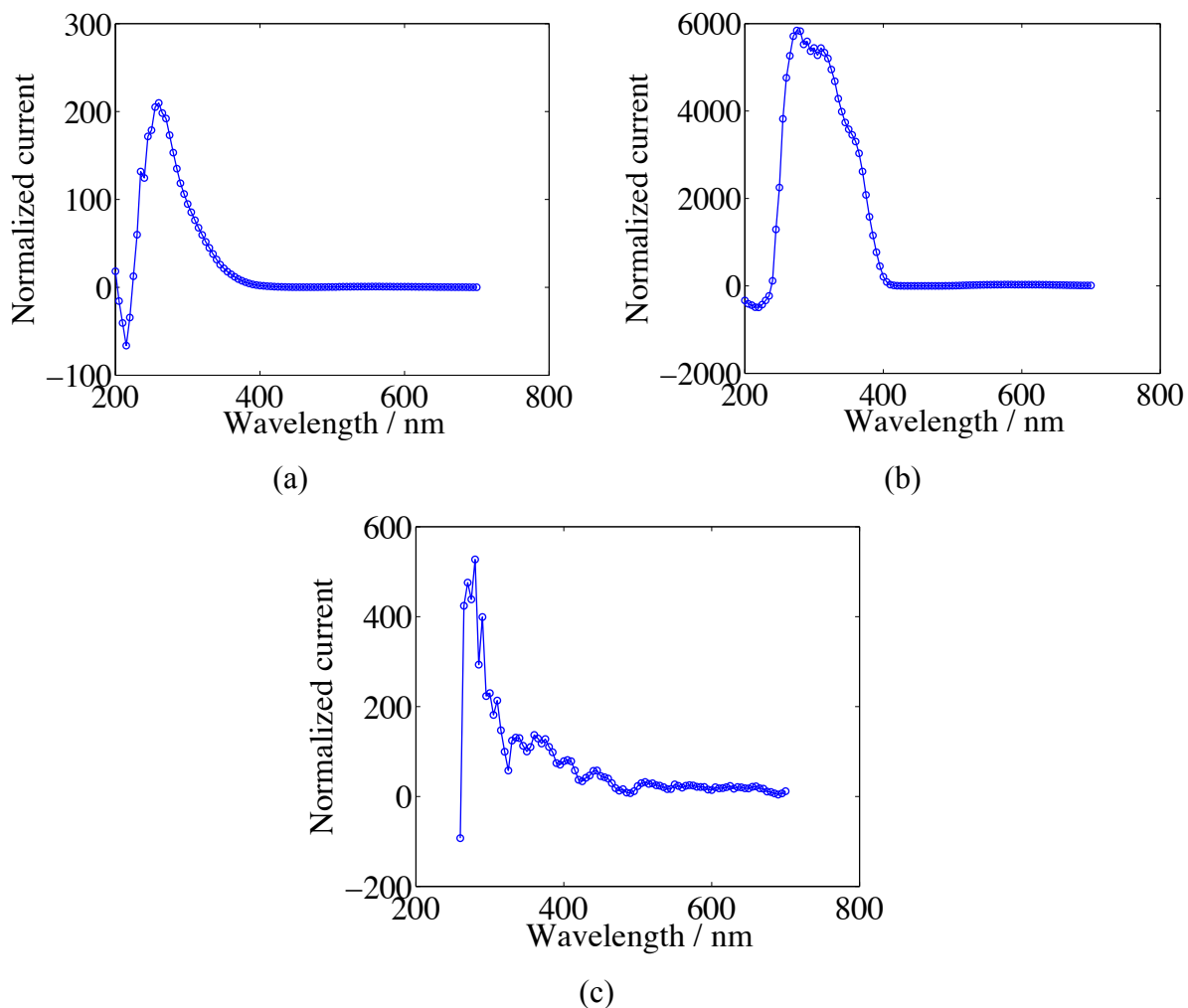
Figure 4.21: Photocurrent recorded for bare ITO-support (a), P 25 on ITO-support (b) and $Ir_{0.4}Sn_{0.6}O_2$ (c). The current is normalized with respect to the intensity of the monochromator and counts the number of electrons per mol photons. (Zahner IMe6 potentiostat)
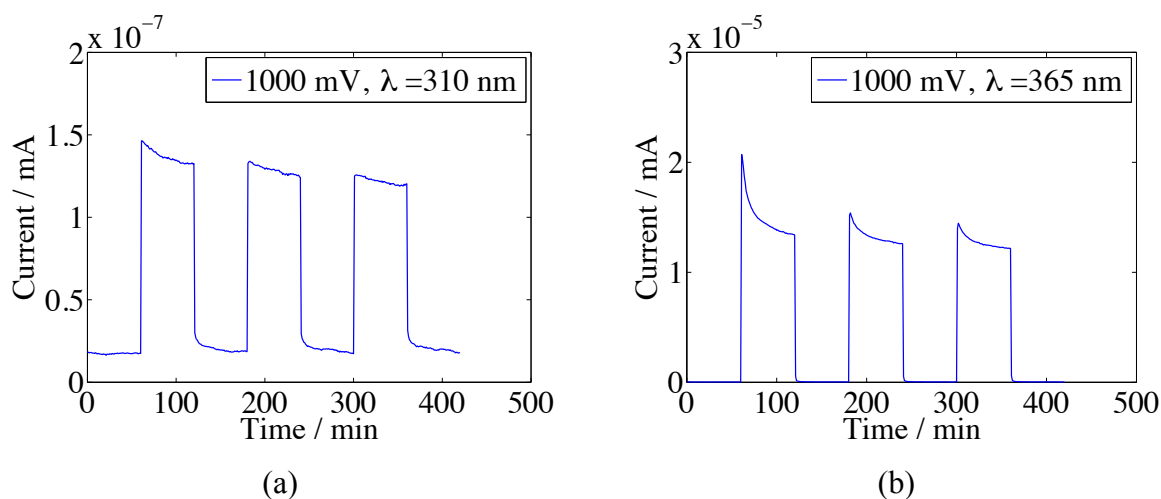
Figure 4.22: Photoresponse for bare ITO (a) and for P25 on ITO (b). Measured using a Zahner IMe6.

4.5 Particle size

The particle size was measured for TiO_2 P25, $Ir_{0.4}Sn_{0.6}O_2$ and $Ir_{0.25}Sn_{0.75}O_2$. A series of three measurements were recorded for each catalyst, with only a couple seconds time delay between each measurement. The recorded size decreased for each measurement for all the tree catalysts. The results are presented in Table 4.4, with an average size calculated from the three measurements.

Table 4.4: Particle size measurements for the catalyst oxides.

	Measurements no.1 (nm)	Measurements no.2 (nm)	Measurements no.3 (nm)	Average particle size (nm)
TiO_2 P25	768.9	666.1	660.0	698.3
$Ir_{0.4}Sn_{0.6}O_2$	584.7	524.0	488.0	532.2
$Ir_{0.25}Sn_{0.75}O_2$	558.6	455.0	425.2	479.6

4.6 An alternative Mott-Schottky analysis

An alternative way to analyze Mott-Schottky behavior for porous electrodes has been derived and the starting point is (2.10) for porous electrodes, repeated here.

$$Z_{porous} = \sqrt{\frac{R_D}{j\omega C_D}} \coth\sqrt{j\omega R_D C_D} \qquad (2.10)$$

The hyperbolic function *coth x = cosh x/sinh x* [16], hence [19]

$$\coth x = \frac{exp(x) + exp(-x)}{exp(x) - exp(-x)} \qquad (4.1)$$

In this case $x = \sqrt{j\omega R_D C_D}$, which means that $\coth\sqrt{j\omega R_D C_D} \rightarrow 1$ at high angular frequencies and allows the simplification of Z_{porous} to

$$\lim_{\omega \to \infty} Z_{porous} \rightarrow \sqrt{\frac{R_D}{j\omega C_D}} \qquad (4.2)$$

By combining the theory for complex numbers [16]

$$\sqrt{\frac{1}{j}} = \sqrt{exp\left(-j\frac{\pi}{2}\right)} = exp\left(-j\frac{\pi}{4}\right) \qquad (4.3)$$

with Eulers formula [19]

$$exp\left(-j\frac{\pi}{4}\right) = \cos\left(-\frac{\pi}{4}\right) + j\,\sin\left(-\frac{\pi}{4}\right) \qquad (4.4)$$

the simplified impedance can be written as

$$Z_{porøs} = \sqrt{\frac{R_D}{j\omega C_D}} = \sqrt{\frac{R_D}{\omega C_D}}\,exp\left(-j\frac{\pi}{4}\right) = \sqrt{\frac{R_D}{\omega C_D}}\cos\left(-\frac{\pi}{4}\right) + \sqrt{\frac{R_D}{\omega C_D}}\,j\sin\left(-\frac{\pi}{4}\right) \qquad (4.5)$$

As can be seen from Eq. (4.5), the imaginary part, *ImZ*, is

$$ImZ = \sin\left(-\frac{\pi}{4}\right)\sqrt{\frac{R_D}{\omega C_D}} = -\frac{1}{2}\sqrt{2}\sqrt{\frac{R_D}{\omega}}\frac{1}{\sqrt{C_D}} \qquad (4.6)$$

The capacitance, C_D, can then be expressed as

$$C_D = \frac{1}{2}\frac{R_D}{\omega}\frac{1}{ImZ^2} \qquad ,where\ \frac{1}{2}\frac{R_D}{\omega} = constant \qquad (4.7)$$

If this holds true, it should be possible to plot an alternative Mott Schottky diagram by plotting ImZ^4 as a function of potential for porous electrodes and obtain Mott Schottky behaviour.

Mott Schottky diagrams for anodized Ti are shown on the left side in Figure 4.23. The diagrams are plotted for frequencies 100 kHz, 10 kHz, 1000 Hz and 100 Hz. The alternative Mott Schottky diagram is shown on the right side for the same frequencies. The regular Mott-Schottky diagrams show slightly curved lines without linear areas. The alternative Mott-Schottky diagram, on the other hand, shows linear areas for both the high and the low frequencies. For an angular frequency of 10 kHz the flatband potential for anodized Ti can be determined to 0.4 V.
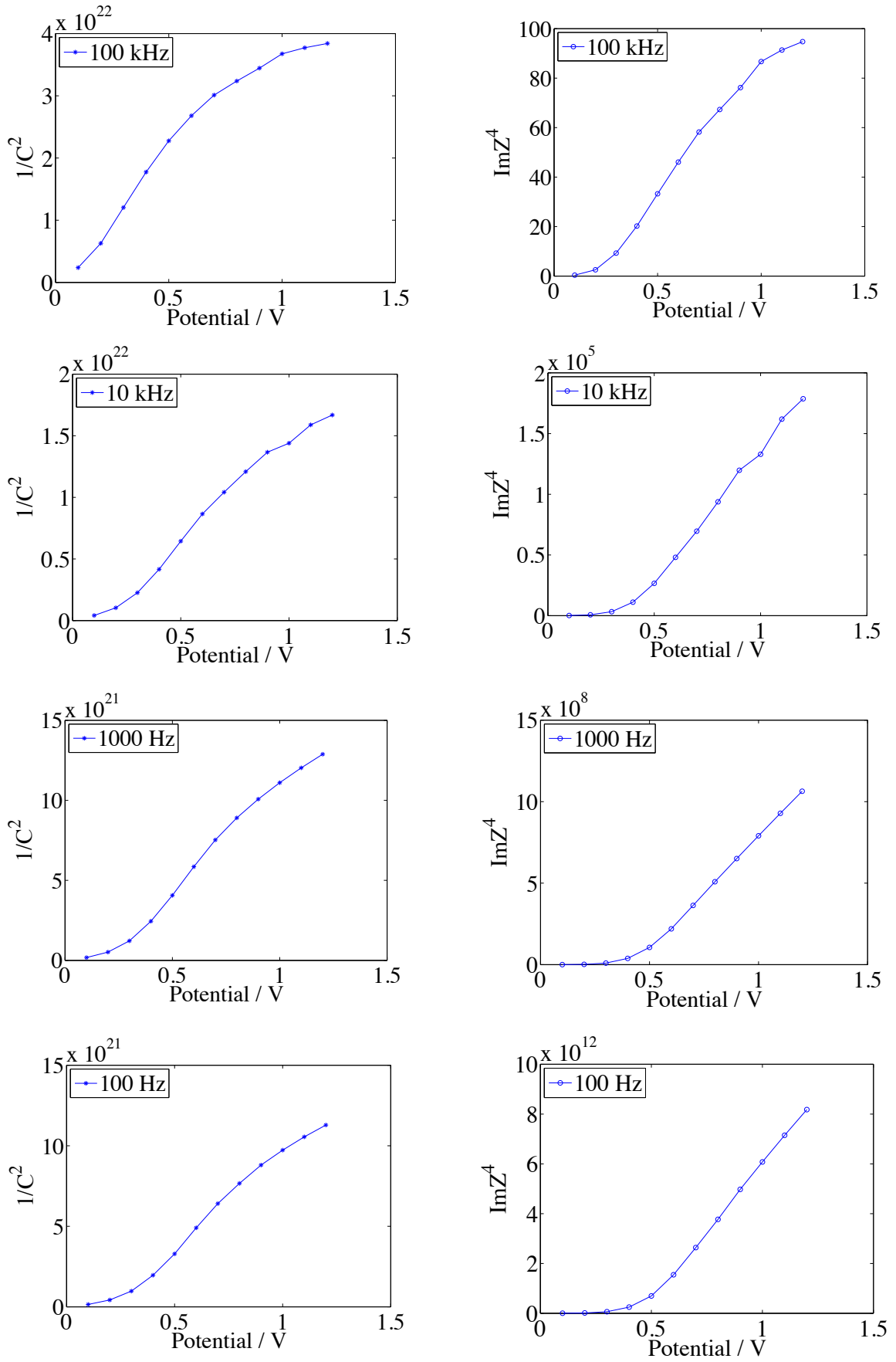
Figure 4.23: Mott Schottky (left) and alternative Mott Schottky plot (right) for anodized Ti.

5   Simulation of the impedance model

5.1   The computer codes

In order to compare the theoretical model and the real response of a porous electrode, a computer code was written. The code is designed to calculate the potential response of a porous semiconductor electrode, according to the equations presented in Chapter 2.3.2.

The original code, calculating the Green's function for the Poisson-Boltzmann problem, was written by Svein Sunde [2]. During this work, the computer code has been extended to include calculation and plotting the dimensionless capacitance, χ.

The computer code consists of several scripts performing different calculations and Table 5.1 lists the computer codes that are used to calculate the non-dimensional capacitance, χ, given in Eq. (2.41). The entire code, viz. the main scripts and the function scripts, can be seen in Appendix A.

5.2   Simulations parameters

The impedance model was simulated using MATLAB® from MathWorks Inc[20]. The parameters chosen for the simulation are given in this section.

The radius of the TiO2 P25 particles is declared by the producer to be about 21 nm [21]. During the experimental work, the particle size for TiO_2 was measured to 698.3 nm. The model is based on the assumption that the particles or agglomerates are large enough to ensure that the Mott-Schottky theory is valid. The width of the depletion region in semiconductors can range from 5 - 500 nm[22] and the higher the doping level, the narrower the region is. From this it is reasonable to set the radius to 350 nm. The charge carrier density for TiO_2 is found to range between 1.0×10^{16} - 1.0×10^{20} cm^{-3} in the literature [23], and 1.5×10^{19} cm^{-3} is reported in[24]. The value of 1.0×10^{16} cm^{-3} corresponds to a lightly doped semiconductor, while 1.0×10^{18} cm^{-3} is considered heavily doped according to [12]. For the simulation of the intrinsic case, n_0 and p_0 is set to 1.0×10^{16} cm^{-3}. The value of n_0 is set to 1.0×10^{17} cm^{-3} in the simulation of the extrinsic case. For highly doped n-type semiconductors, it is reasonable to assume that $n_0 \gg p_0$ and this means that p_0 can be neglected [25].

Table 5.1: Overview of the computer codes used to calculate the non-linear solution to the Poisson-Boltzmanns problem and calculate the non-dimensional capacitence, χ.

PBInt_US.m	Main script for calculating the non-linear solution, u_n, as a function of the dimensionless, x. Calculates the non-dimensional capacitance, χ as a function of the surface potential, u_s.
GreenPB.m	Multiplies the Green's function, G_w, with the charge density, ρ_n.
dGreenPB.m	Multiplies the derivative of the Green's function, dG_w/dx, with the charge density, ρ_n.
GPB.m	Calculates the Green's function for the Poisson Boltzmann equation, G_w.
dGdxPB.m	Calculates the derivative of the Green's function, dG_w/dx.
rhonPB.m	Calculates the charge density, ρ_n.
rhonPB_u.m	Calculates the charge density, $\rho_n(u_s)$, as a function of surface potential.
dGreenPB_u.m	Multiplies the derivative of the Green's function, dG_w/dx, with the charge density, $\rho_n(u_s)$.
rhou.m	Calculates the charge density, $\rho(u_s)$, dependent on surface potential and without the correction term.
dGwrhonPB_u.m	Multiplies the derivative of Green's function, dG_w/dx and $\rho_n(u_s)$.
Heaviside.m	Defines the Heaviside step function.

The dielectric permittivity of TiO_2 is found from the literature to around 55 [24] and 60 [26]. Here it is set to 60. The temperature is set to room temperature, 298 K. A more orderly representation of the parameters is given in Table 5.2 and Table 5.3 for the intrinsic and extrinsic case, respectively. The constants needed for the simulation are listed in Table 5.4

Table 5.2 Parameters used in simulation for intrinsic TiO2.

Parameter	Value	Unit	Reference
R_a	350	nm	See text
n_0	1.0×10^{16}	cm^{-3}	See text
p_0	1.0×10^{16}	cm^{-3}	See text
ε_s	60	-	[26], see text
T	298	K	-

Table 5.3 Parameters used in simulation for extrinsic TiO2.

Parameter	Value	Unit	Reference
R_a	350	nm	See text
n_0	1.0×10^{18}	cm^{-3}	See text
p_0	0	cm^{-3}	See text
ε_s	60	-	[26], see text
T	298	K	-

Table 5.4: The constants used in the simulations.

Constant	Value	Unit	Reference
e	1.602×10^{-19}	C	[27]
ε_0	8.85×10^{-12}	F/m	[27]
k_B	1.38×10^{-23}	J/K	[27]

5.3   Simulation results

5.3.1   Intrinsic case

The intrinsic case was simulated using the parameters in Table 5.2. The potential distribution in the particle, as a function of distance from the center, is shown in Figure 5.1. In this figure, surface potentials ranging from -1.2 V to 1.2 are included. The figure contains three types of markings. The red markings represent the initial, linear solution to the Poisson-Boltzmann problem and the black markings represent the final non-linear solution. The blue lines show the iteration steps. The markings are difficult to discern in this presentation and the potential change for each iteration step is better illustrated in Figure 5.2. This shows the same kind of diagram for a particle size of 100 nm, but here only one surface potential, 1.2 V relative to the flatband potential, is presented. The flatband potential corresponds to a surface potential of zero.
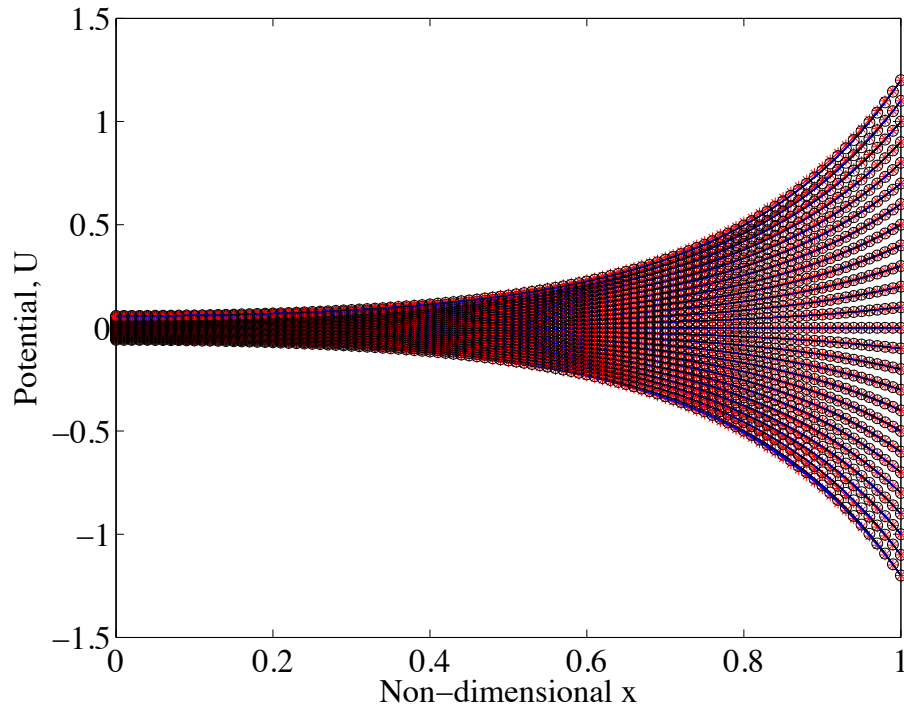
Figure 5.1: The potential distribution as a function of the distance from the center of the particle. The particle radius in this case is 350 nm.
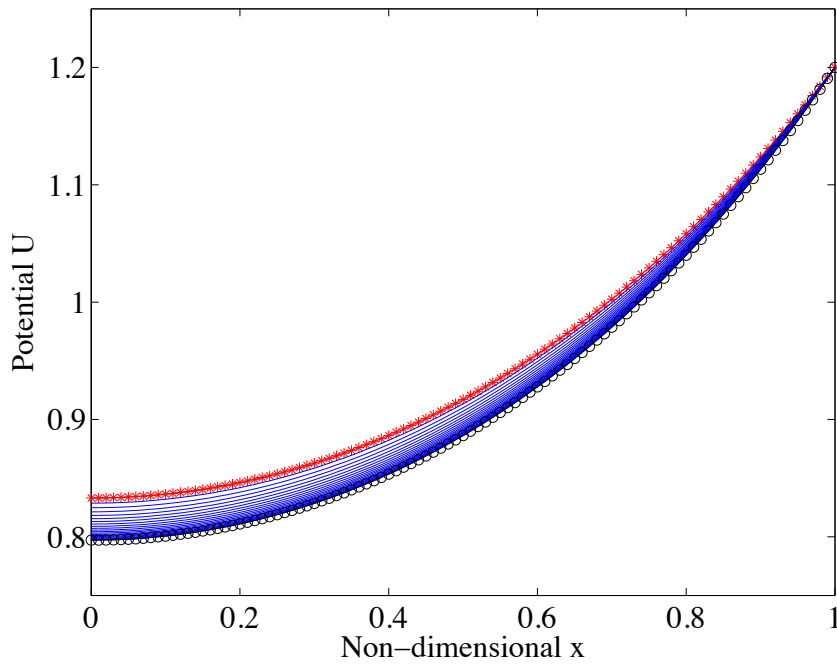
Figure 5.2: The potential distribution in the particle as a function of distance from the center of the particle. The particle radius in this case is 100 nm.

All the following simulations are done using the parameters in Table 5.2. Figure 5.3(a) shows how the charge density changes as a function of the surface potential and dZ/dx, which is proportional to the charge density, is presented in Figure 5.3 (b).

Figure 5.3 (c) shows the linear solution to the Poisson-Boltzmann problem as a function of surface potential, while (d) shows the non-linear part of the solution. For surface potentials of small absolute value, the non-linear solution changes minimally. As the absolute value of the potential increases, the change increases. The sum of the linear and nonlinear part, viz. the total solution to the Poisson-Boltzmann problem is shown in Figure 5.3 (e).

The non-dimensional capacitance as a function of surface potential is presented in Figure 5.4. This figure shows that the capacitance is near constant, regardless of the surface potential, except at the flatband potential. As $u_s \rightarrow 0$ the capacitance approaches zero. Figure 5.5 show the Mott-Schottky diagram calculated using the non-dimensional capacitance. The diagram shows near constant values for most of the surface potentials. At surface potentials close to zero $1/\chi^2 \rightarrow \infty$.
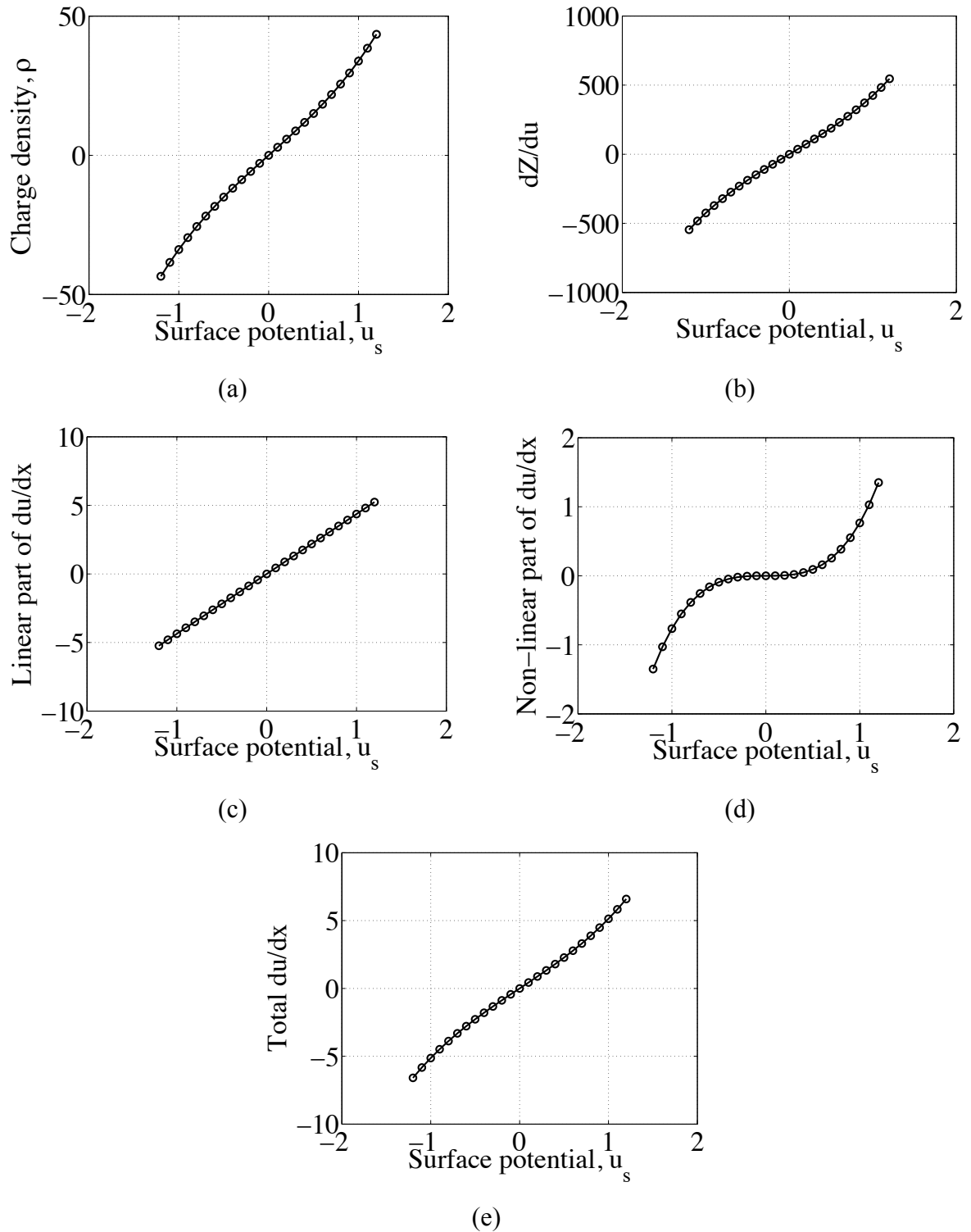
Figure 5.3: The simulated data for the intrinsic case with the parameters given in Table 5.2. (a) The charge density at the surface as a function of surface potential, u_s. (b) The derivative of the charge at the surface as a function of surface potential, u_s. (c) The linear part of the solution of the Poisson-Boltzmann equation, as a function of surface potential, u_s. (d) The non-linear part of the solution to the Poisson-Boltzmann problem. (e) The total solution of the Poisson-Boltzmann equation.
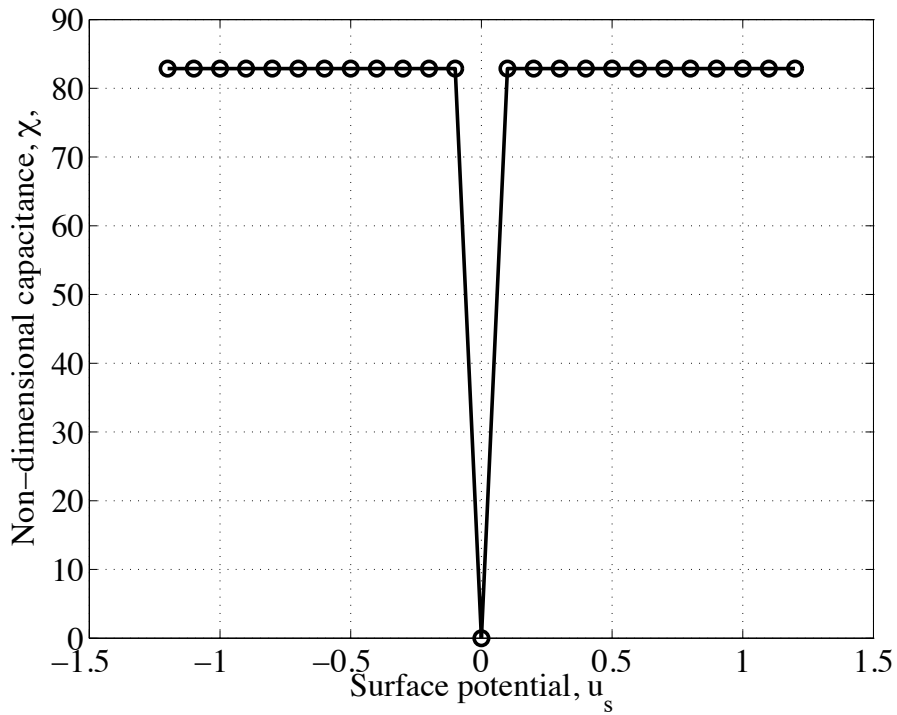
Figure 5.4: The non-dimensional capacitance, χ, as a function of surface potential, u_s, for the intrinsic case.
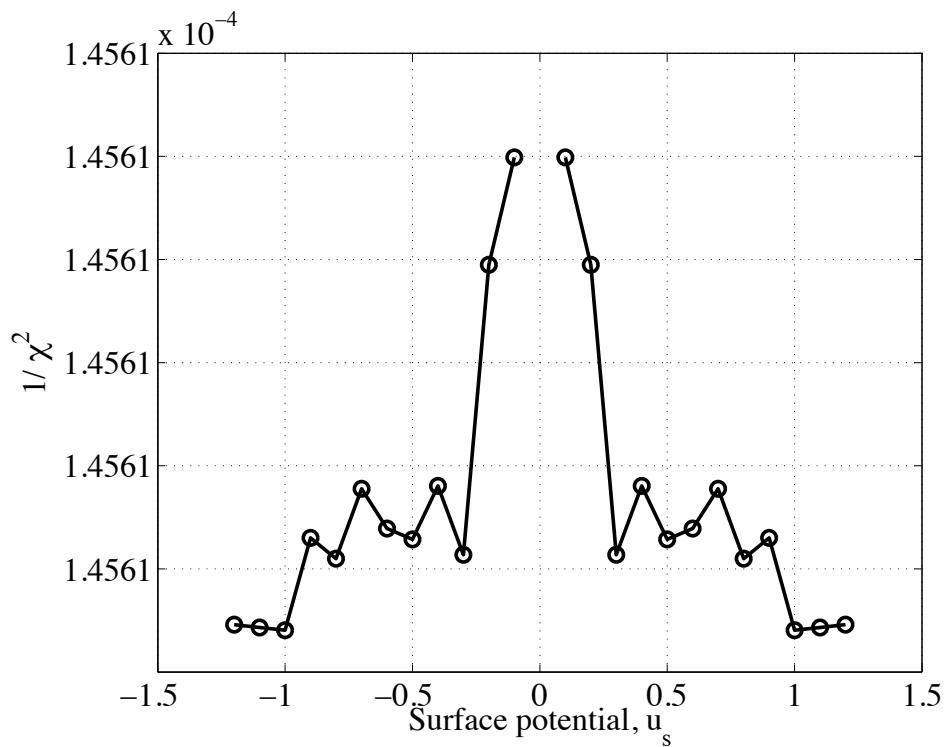
Figure 5.5: The Mott-Schottky diagram plotted using the non-dimensional capacitance for the intrinsic case.

5.3.2 Extrinsic case

The extrinsic case was simulated using the parameters in Table 5.3 and the resulting data is presented here. Figure 5.6 shows the potential distribution as a function of the distance from the particle center. The markings in this figure are the same as described for Figure 5.1.
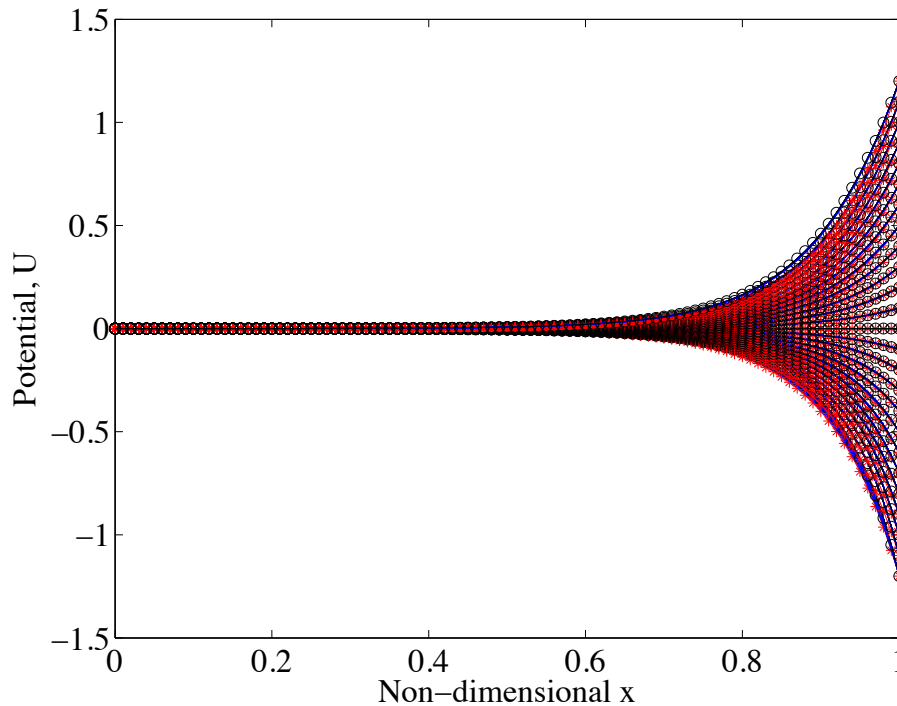
Figure 5.6: The potential distribution as a function of the distance from the center of the particle for the extrinsic case. The particle radius is 350nm.

Figure 5.7 (a) and (b) shows the charge density and dZ/dx as a function of the surface potential, respectively. The linear solution to the Poisson-Boltzmann problem is shown in Figure 5.7 (c) and the nonlinear solution is shown in (d). The total solution, du/dx for the extrinsic case, is presented in Figure 5.7 (e).

The calculated non-dimensional capacitance is presented in Figure 5.8 and the corresponding Mott-Schottky diagram is shown in Figure 5.9. Also in this case, the capacitance is as good as constant for all the surface potentials, except $u_s \rightarrow 0$ where the value goes towards zero. Even though the values in the Mott Schottky diagram looks like they vary the number on the ordinate axis are all the same, which means that the variations are very small.

55
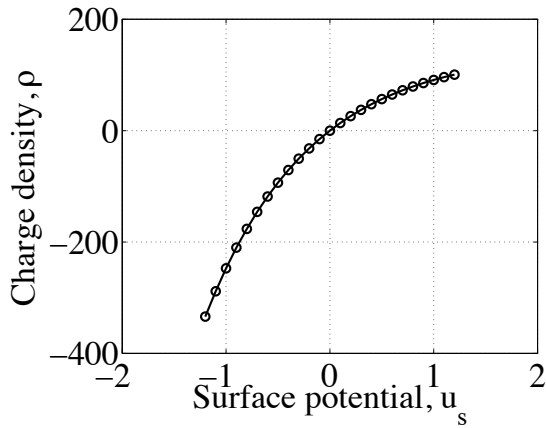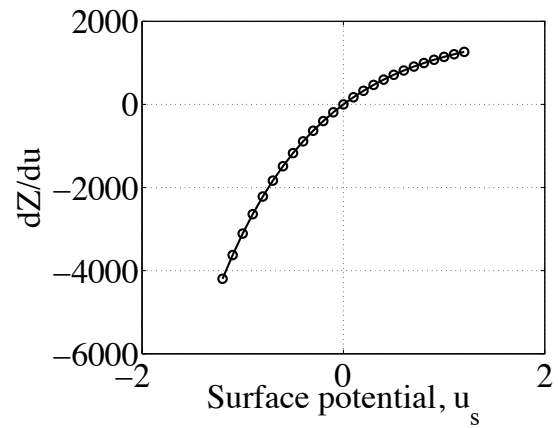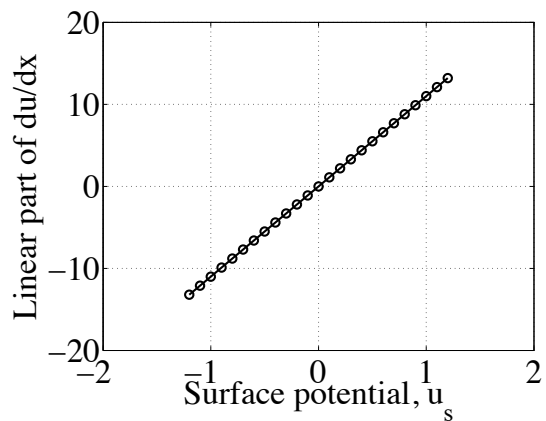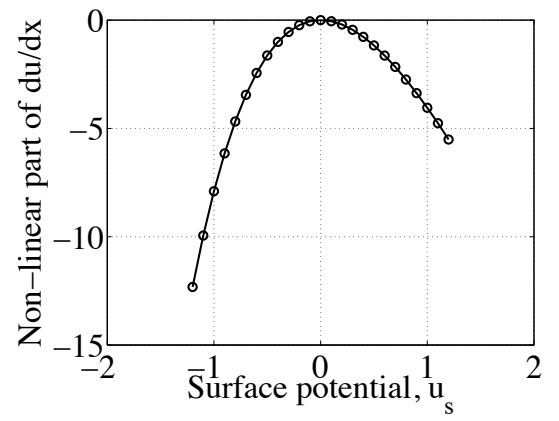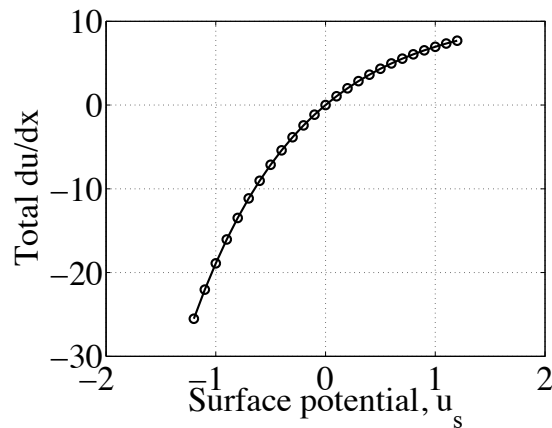
Figure 5.7: The simulated data for the extrinsic case with the parameters given in Table 5.3. (a) The charge density at the surface as a function of surface potential, u_s. (b) The derivative of the charge at the surface as a function of surface potential, u_s. (c) The linear part of the solution of the Poisson-Boltzmann equation, as a function of surface potential, u_s. (d) The non-linear part of the solution to the Poisson-Boltzmann problem. (e) The total solution of the Poisson-Boltzmann equation.
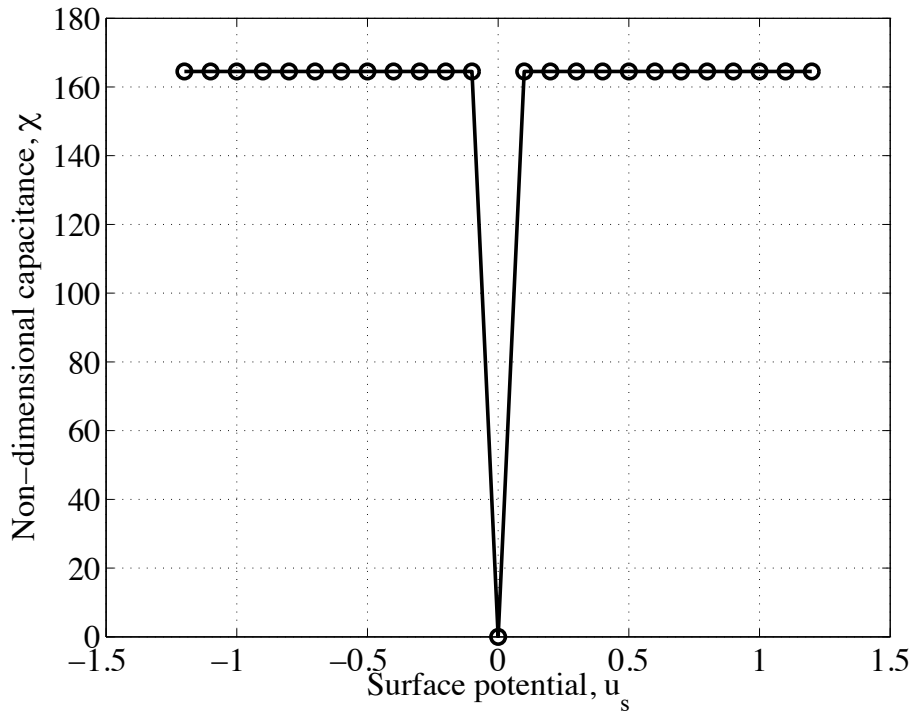
Figure 5.8: The non-dimensional capacitance, χ, as a function of surface potential, u_s, for the extrinsic case.
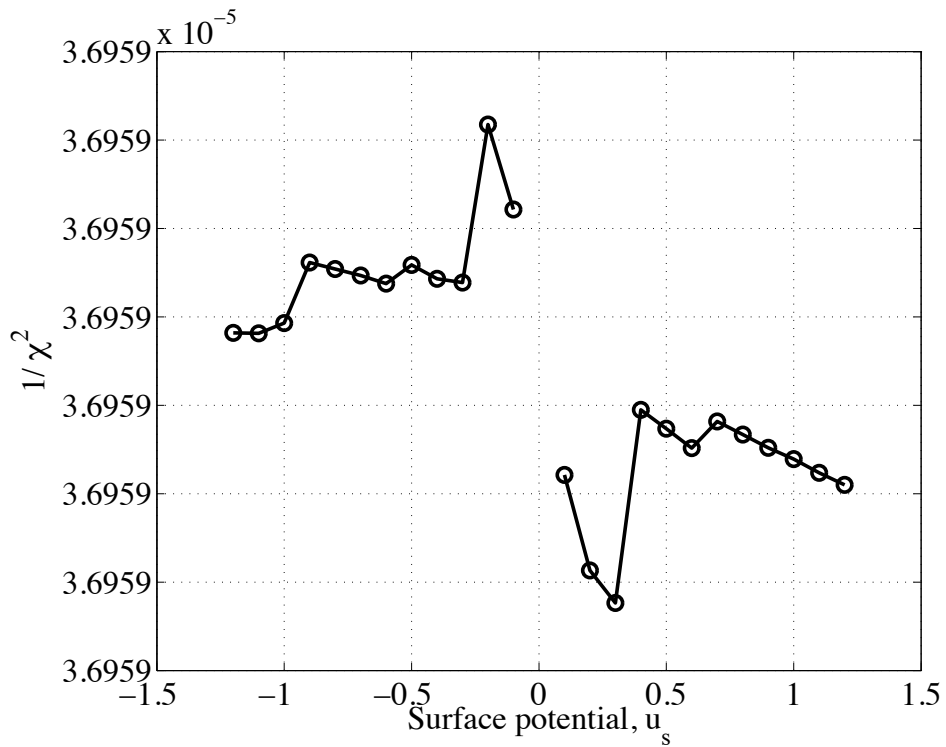
Figure 5.9: The Mott-Schottky diagram for simulation of the extrinsic case, plotted using the non dimensional capacitance.

57

6 Discussion

6.1 Cyclic voltammetry

The recurring challenge when working with powder catalysts it that the substrate is interfering or often dominating the measured results completely. This makes it difficult to study these types of systems and several support materials were tested in during this work.

The Au-support completely dominates the CV for TiO_2 P25, both when Nafion® was mixed in the ink before spraying and when it was dripped onto the film after spraying. The catalyst loading for the P25 Au N-electrode was 8.43 mg/cm^2, which is quite high. The high loading was chosen to ensure good coverage and help adhesion to the support. Unfortunately, the thickness caused the film to crack and a large area of the support was visible to the electrolyte. This was at first suspected to cause the supports dominance. Another concern was that the Nafion®, mixed into the ink, might cause direct contact between the electrolyte and the support and thereby bypassing the oxide particles in the film. The P25 Au Ntop-electrode was made to test this suspicion. The Nafion® was dripped on top of the film to act as a binder and protective layer. The catalyst loading for the P25 Au Ntop-electrode was 1.53 mg/cm^2. Studies of the P25 Au Ntop-electrode in the microscope show an apparently dense film, without cracks and major holes. Nail polish was used to cover the few holes that were found to prevent direct contact between the support and the electrolyte. Despite the new manufacture process, the electrochemical measurements performed on the P25 Au Ntop-electrode reveals about the same degree of interference from the Au-support as the P25 Au N-electrode. From this it seems reasonable to assume that the current does not bypass the catalyst through the Nafion® in the film. However, it might be possible that the sprayed film was dissolved during application of the Nafion® solution in form of droplets. If this is the case, Nafion® might have penetrated into the film to generate contact between the electrolyte and the support also in this case. This has not been confirmed.

The interference of the Au-support seems to be less for iridium tin oxides. The reason for this might be that the iridium tin oxide is more electrocatalytic than both P25 and gold. It is therefore hard to distinguish the interference when cycling the electrodes between 0.0 V and 1.4 V. Au has a very distinctly shaped voltammogram if the anodic turning point is high enough to ensure formation of an oxide layer on the surface, and an anodic turning potential

58

of 1.6 V proved to be sufficient. Cycling between 0.0 V and 1.6 V was done after all the actual experiments were performed because this kind of treatment can damage the oxide films. The shape of the voltammogram for the bare Au-support corresponds to the voltammogram for gold presented by Hamann et al [1]. When comparing the voltammogram for Au-support and the $Ir_{0.4}Sn_{0.6}O_2$ Au-electrode, the characteristic peak for Au can be seen in both curves. Because of this it is not safe to treat the measured data as a response form the oxide catalyst alone.

In an effort to avoid the interference of the support, Ti-plates were tested as a support for P25. To eliminate the questions related to the use of Nafion®, electrode films both with and without Nafion® were tested. Compared to the heat treated Ti 450-electrode, which is the most representative for the electrode supporting the sintered film, the P25 Ti 450-electrode behaves somewhat different. The current measured for potentials between 0.0 V and about 0.2 V is much larger for the sintered film. This indicates that the measured voltammogram is primarily a result of the response of the P25. The general shape of the voltammogram for the sintered film is similar to the voltammogram for the anodized Ti-electrode. This indicates that the sintered film has a structure similar to the anodized Ti. The shape corresponds to results reported in the literature [28, 29] for TiO_2, with a cathodic peak at about 0.05 V. The current measured for the sintered film is larger than the current measured for the anodized film, which is only natural since the resistivity of TiO_2, formed by anodization, increases with the thickness of the film.

ITO was the last support material that was used in the experimental work. For $Ir_{0.25}Sn_{0.75}O_2$ ITO and especially $Ir_{0.4}Sn_{0.6}O_2$ ITO, the shape of the voltammograms are quite different than the voltammogram recorded for bare ITO-substrate. The currents recorded for the oxide electrodes are far larger than that recorded for bare ITO. This indicates that the ITO works well as a support for the iridium tin oxides with the composition used in this work. It is possible that the support influences the measurements to some small degree, in the same way Au does, but upon comparison of the voltammogram for Au-support and ITO-support it can be seen that ITO is far less electrochemically active. From this it is reasonable to assume that the contribution from the support is small enough to be neglected.

This is not the case for the titanium oxide films. The voltammograms for bare ITO and P25 ITO are almost identical in shape and size. This indicates that ITO dominates the measurements of the P25 ITO 450-electrode.

6.2   Electrochemical impedance spectroscopy

The electrochemical impedance measurements performed on P25 with Au-support showed behavior indicating that the support interferes with the measurement. The same results were seen whether Nafion® was used or not. When a powder catalyst is sprayed onto a planar support it is expected, in most cases, that the catalyst film is porous and acts accordingly. Hence, the slope for the logarithmic plot of imaginary part of the impedance, ImZ, and the angular frequency, ω, is expected to be about -1/2. This is at least expected for the high frequency part of the curve, as a porous structure often prevents the signal from penetrating to the bottom of the pores. This was not the case for the P25-electrodes where Au was used as support. The recorded impedance data is almost identical with the corresponding data for the bare Au. All the results point toward the fact that the gold support dominates the measurements performed on the P25 films.

For the iridium tin oxides the Au-support seems to be less dominating. Some of the analysis shows porous behavior, like the Nyquist diagram for $Ir_{0.4}Sn_{0.6}O_2$. However, other analysis proves to be ambiguous, like the Mott-Schottky diagrams for bare Au-support and the $Ir_{0.4}Sn_{0.6}O_2$ Au-electrode. The difference is too small to conclude that the data measured for $Ir_{0.4}Sn_{0.6}O_2$ represents mainly the oxide. Taking into consideration the cyclic voltammograms and the fact that the Au-peak is present in both curves in Figure 1.12, the conclusion is that Au cannot be used as a support when examining these oxides.

The logarithmic plot of ImZ as a function of ω for the P25 Ti N-electrode, P25 Ti 450-electrode and the heat treated Ti-electrode shows that the three electrodes behave in the same way. However, the logarithmic plot of ImZ as a function of ω for the anodized Ti-electrode shows that the electrode behaves as a planar electrode at low frequencies, where the slope of the lines is close to -1. For frequencies higher that 1000 Hz the slope changes to values closer to -1/2. The slope varies from -0.598 to -0.776 depending on the direct potential applied during the recording of the impedance spectrum. The fact that this electrode shows porous

behavior is of great interest with regard to the alternative Mott-Schottky analysis, proposed in Chapter 4.6, but this is discussed in Chapter 6.5.

6.3 Photoelectrochemistry

Photocurrent measurements confirm the semiconductor behavior of all the catalysts used. For ITO, which is a high bandgap semiconductor with E_g = 3.5-4.3 eV[30], the unnormalized data shows a photocurrent that peaks at 310 nm. This corresponds to a bandgap of 4.0 eV, which is well inside the interval given in [30]. The unnormalized data for P25 ITO shows that the current peaks at 365 nm, corresponding to E_g = 3.4 eV. This value is slightly higher that the expected value of 3.2 eV [31, 32]. The normalized data shows that the current recorded during the scan for P25 ITO is about 28 times larger than for bare ITO. Both the ITO-electrode and the P25 ITO-electrode shows rapid photoresponse.

For $Ir_{0.4}Sn_{0.6}O_2$ on ITO the current peak is not as evident as for ITO and P25 ITO. The reason might be that the photoresponse for $Ir_{0.4}Sn_{0.6}O_2$ is found in a previous work[18] to be much slower than for the other two electrodes. However, using the wavelengths where the largest current was recorded yields a bandgap between 2.7-3.4 eV.

6.4 Particle size

Particle size measurements were performed for all the three catalytic oxide powders. The pretreatment of the powder was the same as before spraying the support. This was done to generate measurements that would be representative for the electrodes used in the electrochemical experiments.

The particle size declared by the producer of the TiO_2 P25, as a typical value, is about 21 nm [21]. However, the particle size measured in this project was close to 700 nm. This indicates that the sample used in the particle size measurements contains fairly large agglomerates of smaller TiO_2 particles. The size of the agglomerates could have been reduced by using a mortar to grind them down or by increasing the time the sample spent in the ultrasonic bath. This was not done because the large agglomerate size is seen as an advantage with regard to the analysis of the impedance model. The model assumes particles large enough to sustain the space charge region. The measured average agglomerate size of 698.3 nm should be able to sustain the space charge region in P25 and with regard to this the system is suited as a reference for the simulation of the theoretical model. During the series of measurements the

particle size decreased. The reason could be that the large particles settled as the samples time in the cuvette increased.

For $Ir_{0.4}Sn_{0.6}O_2$ and $Ir_{0.25}Sn_{0.75}O_2$ the average particle/agglomerate size was measured to 532.2 nm and 479.6 nm, respectively. These samples comprises of smaller particles or agglomerates than the P25.

6.5 Alternative Mott-Schottky analysis

The alternative method for analyzing the Mott-Schottky behavior of porous electrodes is confirmed by the impedance measurements performed on anodized Ti. By plotting the original Mott-Schottky plot along side the alternative analysis method the results are striking. While the regular Mott-Schottky diagrams show curved lines with no linear parts, the alternative diagram derived from the impedance for porous electrodes show straight lines. This makes it possible to determine a value for the flatband potential to about 0.4 V, for anodized Ti, in the diagram for ω =10 kHz. This angular frequency is well within the area that shows porous behavior in the logarithmic plot of *ImZ* as a function of ω. The diagrams representing the other frequencies in Figure 1.22 also show a straight line in the alternative Mott-Schottky analysis.

For the electrode films produced by spraying, rather than anodization, the analysis of the Mott-Shottky behavior is not possible to perform in a satisfactory way because of the interferences from the support material. The material that seems to interfere the least is ITO, but the data is still too ambiguous to use as an argument in the discussion about the alternative Mott-Schottky analysis.

6.6 Simulation of the impedance model

The results of the simulations displayed in Chapter 5.3 shows that the potential at the surface changes minimally for each iteration step in the calculation. This seems to be the case both for intrinsic and extrinsic semiconductors and Figure 5.1 and Figure 5.6 shows this. The example for the 100 nm particles in Figure 5.2, shows that the potential in the center of the particles (at *x = 0*) changes considerately more during an iteration step than the surface potential. For the larger particles in the extrinsic case, as shown in Figure 5.6, the potential in the center is approximately constant and the surface potential seems to be close to constant

too. This might indicate that only the potential in the depletion layer is changed during the iterations and that the linear solution dominates outside this layer.

The capacitance in the spherical case seems to be relatively constant regardless of the surface potential. This results in a Mott-Schottky diagram with similar tendencies, although the diagrams in Figure 5.5 and Figure 5.9 gives the impression of relative large differences at first glance. It is important to note that all the numbers on the ordinate axis are the same. The reason for the near constant capacitance is that dZ/dx and du/dx changes at approximately the same rate as the surface potential changes. At this level of analysis, it seems that the spherical system is difficult to analyze using a one-dimensional model.

The results from the alternative Mott-Schottky analysis performed on the anodized Ti shows that the capacitance is strongly dependent on the surface potential. This indicates that the inside of the pores are fairly planar and not spherical as assumed in the impedance model. Because of this it cannot be used to confirm the impedance model.

7 Conclusion

Cyclic voltammetry and electrochemical impedance measurements performed on the oxide electrodes shows that all the support material used in this work, Au, Ti and ITO, interferes with the measurements. In some cases the support clearly dominated the results, as for Au, and in other the results were inconclusive. The measured data for P25, $Ir_{0.4}Sn_{0.6}O_2$ and $Ir_{0.25}Sn_{0.75}O_2$, is therefor not safe to be used as a basis to analyze the impedance model for porous semiconductor electrode.

Photocurrent measurements confirm the semiconducting properties of TiO_2 P25 and $Ir_{0.4}Sn_{0.6}O_2$.

The particle size of TiO_2 P25 was measured to 698.3 nm, which means that the titanium oxide films made in this work comprised of particles or agglomerates of this size. With regard to this, the system should be representative for the impedance model to be analyzed.

The impedance data measured for anodized titanium shows that the oxide film is porous. The results also confirm that the alternative Mott-Schottky theory proposed in this work can be used to analyze the Mott-Schottky behavior for this electrode film.

Simulation of the impedance model for porous semiconductor electrodes shows that the capacitance in electrode films made of spherical particles varies weakly with the surface potential. The reason is that the charge density and the potential in the model vary with approximately the same rate as the surface potential changes. From this it seems that the Mott-Schottky analysis for spherical particles cannot be done using a one-dimensional model.

Bibliography

1. Hamann, C.H., A. Hamnett, and W. Vielstich, *Electrochemistry*, 2007, Wiley: Weinheim. p. 260-286.
2. Sunde, S. and M. Tjelta, *An impedance model for porous semiconductors: Beyond the Mott-Schottky equation*, in *Publication manuscript in preparation 2012, Preprint submitted to Electrochimica Acta*2012.
3. Sunde, S., et al., *An Impedance Model for a Porous Intercalation Electrode with Mixed Conductivity.* Journal of The Electrochemical Society, 2009. **156**(8): p. B927-B937.
4. Schmickler, W. and E. Santos, *Interfacial Electrochemistry*, 2010, Springer-Verlag Berlin Heidelberg: Berlin, Heidelberg. p. 178-185.
5. Greef, R., et al., *Instrumental methods in electrochemistry*, 1990, Ellis Horwood: New York. p. 251-263.
6. Owe, L.-E., *Oxide electocatalyst for the oxygen evolution reaction inwater electrolysis*, 2006, Institutt for materialteknologi, NTNU: Trondheim. p. V, 59 bl.
7. Bruce, P.G., *Solid state electrochemistry*, 1995, Cambridge University Press: Cambridge. p. 264-268.
8. Scholz, F., *Electroanalytical Methods: Guide to Experiments and Applications*, 2010, Springer-Verlag Berlin Heidelberg: Berlin, Heidelberg. p. 159-176.
9. Schlesinger, M. and A. Lasia, *Modeling of Impedance of Porous Electrodes. Modeling and Numerical Simulations*, 2009, Springer New York. p. 67-137.
10. de Levie, R., *On porous electrodes in electrolyte solutions—IV.* Electrochimica Acta, 1964. **9**(9): p. 1231-1245.
11. Sunde, S., G. Hagen, and R. Ødegård, *Impedance analysis of the electrochemical doping of poly(3-methyl-thiophene) from aqueous nitrate solutions.* Journal of Electroanalytical Chemistry, 1993. **345**(1-2): p. 59-82.
12. Krishnan, R., *Fundamentals of Semiconductor Electrochemistry and Photoelectrochemistry*, in *Encyclopedia of Electrochemistry*2007, Wiley-VCH Verlag GmbH & Co. KGaA. p. 1-14.
13. Gelderman, K., L. Lee, and S.W. Donne, *Flat-Band Potential of a Semiconductor: Using the Mott–Schottky Equation.* Journal of Chemical Education, 2007. **84**(4): p. 685-688.
14. Streetman, B.G. and S.K. Banerjee, *Solid State Electronic Devices*2009: Pearson Prentice-Hall. 34-35.
15. Butkov, E., *Mathematical physics*, 1968, Addison-Wesley: Reading, Mass. p. 221-223, 503-508.
16. Stewart, J., *Calculus: early transcendentals*, 2003, Thompson/Brooks/Cole: Belmont, Calif. p. 97, 250, A49-A56.
17. Keener, J.P., *Principles of applied mathematics: transformation and approximation*, 1988, Addison-Wesley: Redwood City, Calif. p. 147-152.
18. Hansen, J.E., *Syntetisering og karakterisering av katalysatorer for vannelektrolyse: Ir(1-x)Sn(x)O2*, 2011: Norwegian University of Science and Technology.
19. Rottmann, K., *Matematisk formelsamling*2003, [Oslo]: Spektrum forl. 176 s.
20. *MATLAB® The Language of Technical Computing*. 2012 [cited 2012 06.18.2012]; Available from: http://www.mathworks.se/products/matlab/.

21. *AEROSIL® and AEROXIDE® for catalyst carrier applications.* [cited 2012 06.09.2012]; Available from: http://www.aerosil.com/product/aerosil/en/effects/photocatalyst/pages/default.aspx.

22. van de Krol, R. and M. Grätzel, *Photoelectrochemical Hydrogen Production*, 2012, Springer US: Boston, MA. p. 33.

23. Sellers, M.C.K. and E.G. Seebauer, *Measurement method for carrier concentration in TiO2 via the Mott–Schottky approach.* Thin Solid Films, 2011. **519**(7): p. 2103-2110.

24. Enache, C.S., J. Schoonman, and R. Van De Krol, *The photoresponse of iron- and carbon-doped TiO2 (anatase) photoelectrodes.* Journal of Electroceramics, 2004. **13**(1-3): p. 177-182.

25. Green, M.A., *Solar cells: operating principles, technology and system applications*, 1992, University of New South Wales: Kensington. p. 30-31.

26. Leroy, P., C. Tournassat, and M. Bizi, *Influence of surface conductivity on the apparent zeta potential of TiO2 nanoparticles.* Journal of Colloid and Interface Science, 2011. **356**(2): p. 442-453.

27. Aylward, G.H. and T.J.V. Findlay, *SI chemical data* 2002, Milton: Wiley. XIV, 202 s.

28. Oliva, F.Y., et al., *Photoelectrochemical characterization of nanocrystalline TiO2 films on titanium substrates.* Journal of Photochemistry and Photobiology A: Chemistry, 2002. **146**(3): p. 175-188.

29. Azumi, K. and M. Seo, *Changes in electrochemical properties of the anodic oxide film formed on titanium during potential sweep.* Corrosion Science, 2001. **43**(3): p. 533-546.

30. Kim, H., et al., *Electrical, optical, and structural properties of indium--tin--oxide thin films for organic light-emitting devices.* Journal of Applied Physics, 1999. **86**(11): p. 6451-6461.

31. Hurum, D.C., et al., *Explaining the Enhanced Photocatalytic Activity of Degussa P25 Mixed-Phase TiO2 Using EPR.* The Journal of Physical Chemistry B, 2003. **107**(19): p. 4545-4549.

32. Stratmann, M. and A.J. Bard, *Encyclopedia of electrochemistry* 2002, Weinheim: Wiley-VCH. 11 b.

Appendix A:

The computer codes
The computer codes used to simulate the impedance model for porous semiconductor electrodes.

PBInt_US.m

```
%*************************************************************************
%                                                                       *
%              SOLUTION OF THE SPHERICAL POISSON-                        *
%              BOLTZMANN EQUATION BASED ON GREEN'S FUNCTION             *
%                                                                       *
%                           Svein Sunde                                 *
%             NTNU, Sem Saelands veg 12, NO-7491 Trondheim             *
%                         Ver. Dec 9, 2011                              *
%                                                                       *
%        Record of revisions:                                           *
%                                                                       *
%        Date         Programmer          Description of change         *
%        ====         ==========          =====================         *
%     16/2/12    Johanna Hansen      Adding menu to choose type of      *
%                                    semiconductor and entering start   *
%                                    conditions                         *
%     07/3/12    Johanna Hansen      Adding calculation of dZ/dx,       *
%                                    dU/dx and capacitance, chi          *
%                                                                       *
%        References:                                                    *
%        [1] James P. Keener, Principles of Applied Mathematics.       *
%            Transformation and approximation,Addison Wesley,          *
%            Redwood City (CA) (1988)                                   *
%                                                                       *
%        Uses:                                                          *
%        GreenPB.m, dGreenPB.m, GPB.m, dGdxPB.m, rhonPB.m, rhonPB_u.m,  *
%        rhou.m, dGwrhonPB.m                                            *
%                                                                       *
%*************************************************************************

% ---- Defining variables -------------------------------------------
%   alpha        --  For successive under-relaxation
%   chi          --  Non dimensional capacitance
%   dGdx         --  Derivative of Green's function
%   dUdx         --  Derivative of the potential, non-linear
%   dZdx         --  Derivative of the charge density
%   e            --  Electron charge, (1.602*10^-19 C)
%   E0           --  Permittivity of free space, (8.85e-12 F/m)
%   Es           --  Dielectric constant of the electrode material
%   fsize        --  Fontsize in figures
%   ftype        --  Fonttype in figures
%   Gw           --  Green's function
%   Gwrhon       --  Product of Greens function and rho_n
%   itmax        --  Number of iterations
%   k            --  Non-dimensional k-value
%   kb           --  Boltzmann's constant, (1,38*10^23 J/K)
%   KNONDIM      --  Non-dimensional k, square root(N0 +P0)
```

I

```
%   n0          --   Concentration of electrons, (1/cm2)
%   N0          --   N0 = (Ra^2*e^2*n0)/(kb*T*Es*E0)
%   name        --   File name data
%   NMESH/nmesh --   Number of data points
%   p0          --   Concentration of holes, (1/cm2)
%   P0          --   P0 = (Ra^2*e^2*p0)/(kb*T*Es*E0)
%   Ra          --   Particle radius, (m)
%   rhon        --   Charge density, (C/cm2)
%   rra         --   Particle radius, (nm)
%   T           --   Temperature (K)
%   u_1         --   Potential, (V) Linear solution to PB.eq.
%   UN          --   Potential, (V) Non-linear solution to PB.eq.
%   UNM1        --   Potential, (V) Linear solution to PB.eq.
%   Unorm       --   Normalized potential
%   US          --   Potential at the particle surface, (V)
%   wn          --   Value of Green's function
%   wnm1        --   Initial value for next iteration of Green's function
%   X           --   Non dimensional radius
%   XNM1        --   Non-dimensional radius
%   dop         --   Doping concentration for naming figures
% -------------------------------------------------------------------


clear
clear all
close all
close all hidden

global US KNONDIM X UNM1 XNM1 N0 P0

% ---- Simulation for n-type TiO2 ------------------------------------

% ---- Set parameters ------------------------------------------------
Ra = 350e-9;                    % Radius of the particles (m)
n0 = 1e23;                      % Charge carrier density, electrons (1/m3)
p0 = 0;                         % Density of holes (1/m3)
Es = 60;                        % Dielectric constant for TiO2
T = 298;                        % Temperature (K)

% ---- Constants -----------------------------------------------------
E0 = 8.85e-12;                  % Permittivity of free space (F/m)
e = 1.602e-19;                  % Charge of electron (C)
kb = 1.38e-23;                  % Boltzmann's constant (J/K)

% ---- Calculating the N0-value --------------------------------------
N0 = (Ra^2 * e^2 * n0)/(kb * T * E0 * Es);
P0 = (Ra^2 * e^2 * p0)/(kb * T * E0 * Es);

% ---- Variables and parameters--------------------------------------
us = -1.2:0.1:1.2;
US = 0;
alpha = 0.1;
NMESH = 100;
itmax = 20;

% ---- Preallocating arrays------------------------------------------
nmesh = NMESH;
X = 0;
XNM1 = zeros(nmesh+1,1);
UNM1 = zeros(length(XNM1),1);
UN = UNM1;
Gwrhon = UNM1;
```

II

```matlab
wnm1 = UNM1;
rhon = UNM1;
wn = UNM1;
dGdx = zeros(1,length(XNM1));
Gw = dGdx;
dZdx = zeros(length(us),1);
dUdx = zeros(length(us),1);
dUdx_lin = zeros(length(us),1);
dUdx_nonlin = zeros(length(us),1);
chi = zeros(length(us),1);
chi_ms = zeros(length(us),1);
rhon_u = zeros(length(us),1);
rho_u = zeros(length(us),1);

% ---- Setting figure properties --------------------------------------
rra = Ra * 1e9;
psize = num2str(rra);
if n0 == 1e22
dop = '1e22m3';
elseif n0 == 1e23
    dop = '1e23m3';
elseif n0 == 1e24
    dop = '1e24m3';
elseif n0 == 1e25
    dop = '1e25m3';
elseif n0 == 1e26
    dop = '1e26m3';
end

name = strcat('TEST_10to10_extrinsic_size_',psize,'nm_','n0_p0_',dop);

fsize = 32;
ftype = 'Times';
point = 8;
lsize = 2;

% ---- Generate figure and calculate non-linear solution ------------------

hf1 = figure(1);
axes('FontSize',fsize,'FontName',ftype);
hold all;

for ius = 1:length(us); % Loop over ius number of surface potentials ------

    % ---- Calculate non-dimensional k:---------------------------------
    KNONDIM = sqrt(P0+N0);
    k = KNONDIM;

    % Array of US: ------------------------------------------------------
    US = us(ius);

    %Initial approximation for unm1:-----------------------------------
    for i=1:nmesh+1
        XNM1(i) = (i-1)/nmesh;
        if i > 1
            UNM1(i) = US*sinh(k*XNM1(i))/(XNM1(i)*sinh(k));
        else
            UNM1(i) = US*k*cosh(k*XNM1(i))/sinh(k); %L'H?pital limit
                                                    %for x -> 0.;
        end
```

III

```matlab
    end

    u_l = UNM1;                          % Linear solution = homogeneous solution

    norm = 1e30;

    grid off;
    box on;

    xlabel('Non-dimensional x','FontSize',fsize,'FontName',ftype);
    ylabel('Potential, U','FontSize',fsize,'FontName',ftype);
    hold all;
    plot(XNM1,UNM1,'color','r','marker','*');

    for i=1:itmax

        for j=1:nmesh+1
            X = XNM1(j);  % x in the integral over the Green's function
            if abs(XNM1(j)) > 1.e-6
                wn(j) = alpha*quad(@GreenPB,0,1)+(1-alpha)*wnm1(j);
                %Integrate over xi
                UN(j) = u_l(j) + wn(j)/X;% [1] p. 159
            else
                wn(j) = quad(@dGreenPB,0,1);%Integrate over xi.
                wn(j) = alpha * wn(j) + (1-alpha) * wnm1(j);
                UN(j) = u_l(j) + wn(j);%See [1] p. 159 and L'Hopital
            end
        end
        plot(XNM1,UN,'color','b');
        if min(UN) < max(UN)
        end
        if abs(UN'*UN) > 1.e-6
            norm = sqrt((UN-UNM1)'*(UN-UNM1))/(UN'* UN);
            %Relative change in this iteration
        else
            norm = sqrt((UN-UNM1)'*(UN-UNM1));
        end
    %       pause(1)
        if norm < 1.e-6
            %Converged!
            break
        end
%        Unorm(ius,i) = (UN-UNM1)' * (UN-UNM1);
        UNM1 = UN;
        wnm1 = wn;%Previous w_{n-1}

    end
    plot(XNM1,UN,'color','k','marker','o');


    % ---- Calculate the non-dimensional capacitance ---------------------
    rhon_u(ius) = rhonPB_u(US);
    rho_u(ius) = rhou(US);
    dZdx(ius) = 4 * pi * (rhou(US)); % Here x = 1 (surface)

    dUdx(ius) = (us(ius)*((k*cosh(k)-sinh(k))/(sinh(k))))...
        - (alpha*quad(@GreenPB_u,0,1)+(1-alpha)*wnm1(j))...
        + quad(@dGwrhonPB,0,1);
    dUdx_lin(ius) = (us(ius)*((k*cosh(k)-sinh(k))/(sinh(k))));
    dUdx_nonlin(ius) = -(alpha*quad(@GreenPB_u,0,1)+(1-alpha)*wnm1(j))...
```

IV

```matlab
        + quad(@dGwrhonPB,0,1);

    chi(ius) = dZdx(ius)/dUdx(ius);
    chi_ms(ius) = 1/(chi(ius))^2;

end


% ---- Saves figure 1 as PDF --------------------------------------
set(hf1,'PaperPositionMode','auto');
saveas(hf1,['Pot_vs_xnm_' name],'pdf');

% ---- Plots du/dx ------------------------------------------------
hf2 = figure(2);
axes('FontSize',fsize,'FontName','Times');
grid on;
box on;
xlabel('Surface potential, u_s','FontSize',fsize,'FontName',ftype);
ylabel('Total du/dx','FontSize',fsize,'FontName',ftype);
hold all;
plot(us,dUdx,'-o','color','k','MarkerSize',point,'LineWidth',lsize);

set(hf2,'PaperPositionMode','auto');
saveas(hf2,['dudx_usurf_' name],'pdf');

% ---- Plots linear part of du/dx ---------------------------------
hf3 = figure(3);
axes('FontSize',fsize','FontName','Times');
grid on;
box on;
xlabel('Surface potential, u_s','FontSize',fsize,'FontName',ftype);
ylabel('Linear part of du/dx','FontSize',fsize,'FontName',ftype);
hold all;
plot(us,dUdx_lin,'-o','color','k','MarkerSize',point,'LineWidth',lsize);

set(hf3,'PaperPositionMode','auto');
saveas(hf3,['Lindudx_usurf_' name],'pdf');

% ---- Plots non-linear part of du/dx -----------------------------
hf4 = figure(4);
axes('FontSize',fsize','FontName','Times');
grid on;
box on;
xlabel('Surface potential, u_s','FontSize',fsize,'FontName',ftype);
ylabel('Non-linear part of du/dx','FontSize',fsize,...
    'FontName',ftype);
hold all;
plot(us,dUdx_nonlin,'-o','color','k','MarkerSize',point,'LineWidth',lsize);

set(hf4,'PaperPositionMode','auto');
saveas(hf4,['Nonlindudx_usurf' name],'pdf');

% ---- Plots rho_n as a function of Us ----------------------------
hf5 = figure(5);
axes('FontSize',fsize','FontName','Times');
grid on;
box on;
xlabel('Surface potential, u_s','FontSize',fsize,'FontName',ftype);
ylabel('Charge density, \rho','FontSize',fsize,'FontName',ftype);
hold all;
plot(us,rho_u,'-o','color','k','MarkerSize',point,'LineWidth',lsize);
```

V

```matlab
set(hf5,'PaperPositionMode','auto');
saveas(hf5,['Chardens_usurf_' name],'pdf');

% ---- Plots capacitance ----------------------------------------------
hf6 = figure(6);
axes('FontSize',fsize','FontName','Times');
grid on;
box on;
xlabel('Surface potential, u_s','FontSize',fsize,'FontName',ftype);
ylabel('Non-dimensional capacitance, \chi','FontSize',fsize,...
    'FontName',ftype);
hold all;
plot(us,chi,'-o','color','k','MarkerSize',point,'LineWidth',lsize);

set(hf6,'PaperPositionMode','auto');
saveas(hf6,['Cap_usurf_' name],'pdf');

% ---- Plots MS -------------------------------------------------------
hf7 = figure(7);
axes('FontSize',fsize,'FontName','Times');
grid on;
box on;
xlabel('Surface potential, u_s','FontSize',fsize,'FontName',ftype);
ylabel('1/ \chi^2','FontSize',fsize,'FontName',ftype);
hold all;
plot(us,chi_ms,'-o','color','k','MarkerSize',point,'LineWidth',lsize);

set(hf7,'PaperPositionMode','auto');
saveas(hf7,['MS_usurf_' name],'pdf');

% ---- Plots dz/dx ----------------------------------------------------
hf8 = figure(8);
axes('FontSize',fsize,'FontName','Times');
grid on;
box on;
xlabel('Surface potential, u_s','FontSize',fsize,'FontName',ftype);
ylabel('dZ/du','FontSize',fsize,'FontName',ftype);
hold all;
plot(us,dZdx,'-o','color','k','MarkerSize',point,'LineWidth',lsize);

set(hf8,'PaperPositionMode','auto');
saveas(hf8,['dZdx_usurf_' name],'pdf');
```

GPB.m

```matlab
%************************************************************************
%                                                                      *
%              GREEN'S FUNCTION FOR THE SPHERICAL POISSON-             *
%              BOLTZMANN EQUATION                                       *
%                                                                      *
%                          Svein Sunde                                 *
%              NTNU, Sem Saelands veg 12, NO-7491 Trondheim            *
%                         Ver. Dec 9, 2011                             *
%                                                                      *
%       Uses: Heaviside.m                                              *
%                                                                      *
%************************************************************************
function [Gw] = GPB(x,xi)

    global US KNONDIM X UNM1 XNM1 N0 P0

    k = KNONDIM;

    if abs(xi) > 1.e-6
        Gw =(cosh(k * (x + xi - 1)) ...
            - cosh(k * (x - xi - 1))) / (2 * k * xi * sinh(k)) ...
            - Heaviside(xi - x) * sinh(k * (x - xi)) / (k * xi);
    else
        Gw = sinh(k * (x - 1)) / sinh(k) + (1 - Heaviside(x));
    end
return
end
```

rhonPB.m

```matlab
%************************************************************************
%                                                                      *
%              GREEN'S FUNCTION FOR THE SPHERICAL POISSON-             *
%              BOLTZMANN EQUATION                                       *
%                                                                      *
%                          Svein Sunde                                 *
%              NTNU, Sem Saelands veg 12, NO-7491 Trondheim            *
%                         Ver. Dec 9, 2011                             *
%                                                                      *
%       Uses: interpl.m                                                *
%                                                                      *
%************************************************************************
function [rhon] = rhonPB(x)

    global US KNONDIM X UNM1 XNM1 N0 P0

    k = KNONDIM;
    u = interp1(XNM1,UNM1,x,'spline');

    rhon = N0 - P0 - N0 * exp(-u) + P0 * exp(u) - k^2*u;
    rhon = rhon * x^2;%Spherical integration: Multiply with r^2 dr
return
end
```

GreenPB.m

```matlab
%*************************************************************************
%                                                                       *
%               GREEN'S FUNCTION FOR THE SPHERICAL POISSON-             *
%               BOLTZMANN EQUATION                                       *
%                                                                       *
%                          Svein Sunde                                   *
%               NTNU, Sem Saelands veg 12, NO-7491 Trondheim            *
%                          Ver. Dec 9, 2011                             *
%                                                                       *
%        Uses: GPB.m  rhonPB.m  interpl.m                               *
%                                                                       *
%*************************************************************************
function [Gwrhon] = GreenPB(xi)

    global US KNONDIM X UNM1 XNM1 N0 P0

    k = KNONDIM;
    x = X;
    u = interp1(XNM1,UNM1,xi,'spline');

    for i=1:length(xi)
        Gw = GPB(x,xi(i));
        rhon = rhonPB(xi(i));
        Gwrhon(i) = Gw*rhon;
    end
return
end
```

dGdxPB.m

```matlab
%*************************************************************************
%                                                                       *
%               GREEN'S FUNCTION FOR THE SPHERICAL POISSON-             *
%               BOLTZMANN EQUATION                                       *
%                                                                       *
%                          Svein Sunde                                   *
%               NTNU, Sem Saelands veg 12, NO-7491 Trondheim            *
%                          Ver. Dec 9, 2011                             *
%                                                                       *
%        Uses: Heaviside.m                                               *
%                                                                       *
%*************************************************************************
function [dGdx] = dGdxPB(x,xi)

    global US KNONDIM X UNM1 XNM1 N0 P0

    k = KNONDIM;

    if abs(xi) > 1.e-6
        dGdx = (sinh(k * (x + xi - 1)) ...
                - sinh(k * (x - xi - 1))) / (2 * xi * sinh(k)) ...
                - Heaviside(xi - x) * cosh(k * (x - xi)) / xi;
    else
        dGdx = k * cosh(k * (x - 1)) / sinh(k);
        % Note that the integral of a delta-function x charge density must
        % be added explicitely outside this routine
    end
return
end
```

dGreenPB.m

```matlab
%**************************************************************************
%                                                                        *
%              GREEN'S FUNCTION FOR THE SPHERICAL POISSON-               *
%              BOLTZMANN EQUATION                                         *
%                                                                        *
%                          Svein Sunde                                    *
%              NTNU, Sem Saelands veg 12, NO-7491 Trondheim              *
%                        Ver. Dec 9, 2011                                 *
%                                                                        *
%       Uses: dGdxPB.m, rhonPB.m, interpl.m                              *
%                                                                        *
%**************************************************************************
function [dGdxrhon] = dGreenPB(xi)

    global US KNONDIM X UNM1 XNM1 N0 P0

    k = KNONDIM;
    x = X;
    u = interp1(XNM1,UNM1,xi,'spline');

    for i=1:length(xi)
        dGdx = dGdxPB(x,xi(i));
        rhon = rhonPB(xi(i));
        dGdxrhon(i) = dGdx*rhon;
    end
return
end
```

rhonPB_u.m

```matlab
%**************************************************************************
%                                                                        *
%              GREEN'S FUNCTION FOR THE SPHERICAL POISSON-               *
%              BOLTZMANN EQUATION                                         *
%                                                                        *
%                          Svein Sunde                                    *
%              NTNU, Sem Saelands veg 12, NO-7491 Trondheim              *
%                        Ver. Dec 9, 2011                                 *
%                                                                        *
%       Date       Programmer          Description of change             *
%       ----       ----------          ---------------------             *
%     26/05/12   Johanna Hansen        Calculate as a function of        *
%                                      surface potential instead of      *
%                                      potential u(x)                     *
%                                                                        *
%**************************************************************************
function [rhon_u] = rhonPB_u(us)

    global US KNONDIM X UNM1 XNM1 N0 P0

    k = KNONDIM;

    rhon_u = N0 - P0 - N0 * exp(-us) + P0 * exp(us) - k^2*us;
return
end
```

dGreenPB_u.m

```matlab
%************************************************************************
%                                                                      *
%               GREEN'S FUNCTION FOR THE SPHERICAL POISSON-            *
%               BOLTZMANN EQUATION                                     *
%                                                                      *
%                          Svein Sunde                                 *
%               NTNU, Sem Saelands veg 12, NO-7491 Trondheim           *
%                          Ver. Dec 9, 2011                            *
%                                                                      *
%        Record of revisions:                                          *
%                                                                      *
%        Date          Programmer           Description of change      *
%        ====          ==========           =====================      *
%     07/3/12    Johanna Hansen              Changing scrifp to use rhonPB_u.m *
%                                            instead of rhonPB.m        *
%                                                                      *
%        Uses: GPB.m, rhonPB_u.m                                       *
%                                                                      *
%************************************************************************
function [dGdxrhon] = dGreenPB_u(xi)

    global US KNONDIM X UNM1 XNM1 N0 P0

    k = KNONDIM;
    us = US;
    x = X;
    rhon = rhonPB_u(us);

    for i=1:length(xi)
        dGdx = dGdxPB(x,xi(i));
        dGdxrhon(i) = dGdx*rhon;
    end
return
end
```

rhou.m

```matlab
%************************************************************************
%                                                                      *
%               GREEN'S FUNCTION FOR THE SPHERICAL POISSON-            *
%               BOLTZMANN EQUATION                                     *
%                                                                      *
%        Date          Programmer           Description of change      *
%        ----          ----------           --------------------       *
%     26/05/12   Johanna Hansen             Original code              *
%                                                                      *
%************************************************************************
function [rho_u] = rhonPB_u(us)

    global US KNONDIM X UNM1 XNM1 N0 P0

    k = KNONDIM;

    rho_u = N0 - P0 - N0 * exp(-us) + P0 * exp(us);
return
end
```

X

dGwrhonPB_u.m

```
%************************************************************************
%                                                                      *
%              GREEN'S FUNCTION FOR THE SPHERICAL POISSON-             *
%              BOLTZMANN EQUATION                                       *
%                                                                      *
%         Date        Programmer            Description of change      *
%         ----        ----------            ---------------------      *
%         26/05/12   Johanna Hansen          Original code             *
%                                                                      *
%************************************************************************
function [dGwrhon] = dGwrhonPB_u(xi)

    global US KNONDIM X UNM1 XNM1 N0 P0

    us = US;
    rhon = rhonPB_u(us);

    for i=1:length(xi)
        dGwdx = dGdxPB(1,xi(i));
        dGwrhon(i) = (dGwdx * rhon) * (xi(i))^2;
    end
return
end
```

Heaviside.m
```
function [Heaviside] = Heaviside(x)
%Heaviside's step function
    if x <= 0
        Heaviside = 0;
    else
        Heaviside = 1;
    end
end
```